Title: Structural epitope profiling identifies antibodies associated with critical COVID-19 and long COVID

Authors: Patrick K.A. Kearns[1,2]*, Charles Dixon[1†], Mihaly Badonyi[1†], Kim Lee[3], Rafal Czapiewski[1], Olivia Fleming[1], Lukas Gerasimivicous[1], Rinal Sahputra[4], Bethany Potts[4], Sam Benton[3], Jacky Guy[5], Scott Neilson[6], Helen Wise[7], Sara Jenks[7], Kate Templeton[7], Tracy Hussell[4], CIRCO[4], Christina Dold[8], Teresa Lambe[8], Alexander J Mentzer[9], Julian C Knight[9], Andrew Pollard[8], COMBAT[9], Susanna Dunachie[10,11,12,13], Paul Klenerman[10,12,14,15], Eleanor Barnes[10,12,14,15], Alan Carson[2], Laura McWhirter[2], Rennos Fragkoudis[5], Susan Rosser[5], David Cavanagh[3], Madhvi Menon[4], Joseph A. Marsh[1], Dirk A. Kleinjan[5], Nick Gilbert[1]*

Affiliations:

[1]MRC Human Genetics Unit, Institute of Genetics and Cancer, University of Edinburgh; Western General Hospital. Crewe Road, Edinburgh EH4 2XU.

[2]Centre for Clinical Brain Sciences, University of Edinburgh; 49 Little France Crescent, Edinburgh, United Kingdom EH16 4SB.

[3]Institute of Immunology and Infection Research, School of Biological Sciences, University of Edinburgh; The King's Buildings, Ashworth Laboratories, Charlotte Auerbach Road, Edinburgh, EH9 3FL.

[4]Lydia Becker Institute, Division of Infection, Immunity & Respiratory Medicine, School of Biological Sciences, University of Manchester; Oxford Rd, Manchester, United Kingdom M13 9PL.

[5]Centre for Synthetic and Systems Biology, School of Biological Sciences, University of Edinburgh; CH Waddington Building, Kings Buildings, Mayfield Road, Edinburgh EH9 3JD.

[6]Edinburgh Genome Foundry, University of Edinburgh; Michael Swann Building, Max Born Crescent, Edinburgh, United Kingdom EH9 3BF.

[7]Department of Clinical Biochemistry, Royal Infirmary of Edinburgh; 51 Little France Cres, Old Dalkeith Rd, Edinburgh, United Kingdom EH16 4SA.

[8]Oxford Vaccine Group, Centre for Clinical Vaccinology and Tropical Medicine, University of Oxford; Churchill Hospital Old Road, Headington, Oxford, United Kingdom OX3 7LE.

[9]Wellcome Centre for Human Genetics, Nuffield Department of Medicine, University of Oxford, Roosevelt Drive, Oxford, United Kingdom OX3 7BN.

[10]Peter Medawar Building for Pathogen Research, Nuffield Dept. of Clinical Medicine, University of Oxford, UK

[11]Oxford Centre for Global Health Research, Nuffield Dept. of Clinical Medicine, University of Oxford, UK

[12]Oxford University Hospitals NHS Foundation Trust, Oxford, UK

[13]Mahidol-Oxford Tropical Medicine Research Unit, Bangkok, Thailand

[14]NIHR Oxford Biomedical Research Centre, University of Oxford, Oxford, UK

[15]Translational Gastroenterology Unit, University of Oxford, UK

*Corresponding authors. Email: P.Kearns@ed.ac.uk; Nick.Gilbert@ed.ac.uk.

†These authors contributed equally.

Abstract: Antibodies can have beneficial, neutral, or harmful effects so resolving an antibody repertoire to its target epitopes may explain heterogeneity in susceptibility to infectious disease. However, the three-dimensional nature of antibody-epitope interactions limits discovery of important targets. We describe and experimentally validated a novel computational method and synthetic biology pipeline for identifying epitopes that are structurally stable and functionally important and apply it to the SARS-CoV-2 proteome. We show patterns of epitope-binding antibodies associated with immunopathology, including a non-isotype switching IgM response to a Membrane protein epitope which is amongst the strongest immunological features associated with severe COVID-19 to date (adjusted OR 72.14, 95% CI: 9.71 – 1300.15). Consistent with a hypothesis that the mechanism driving the non-switching response was T independent B cell activation, we find that B cells secrete IgM and proliferate on exposure to virus-like particles lacking Spike. We also identified persistence (> 1 year) of this response in individuals with longCOVID particularly affected by fatigue and depression. These findings point to a previously unrecognized coronavirus host-pathogen interaction. We demonstrate that the Membrane epitope is a promising vaccine and monoclonal antibody target, which may complement spike-directed vaccination broadening immunological protection.

One-Sentence Summary: Using a protein-structure-based B cell epitope discovery method with a wide range of possible applications, we have identified a novel host-pathogen signature associated with SARS-CoV-2 immunopathology and suggest the viral Membrane protein contains a pathological T independent antigen.

Main Text:

Most vertebrates acquire remarkably heterogeneous repertoires of antibody-secreting cells after encountering a pathogen (*1*). B cells are selected for the affinity of their membrane-bound immunoglobulin receptor (mIg) to bind surfaces (epitopes) on foreign materials (e.g. viral proteins), and high-affinity clones are activated, expanded and differentiate to secrete matching antibodies into blood and mucosa (*2*). Anti-viral immunoglobulin binding may be functionally useful, for example, neutralising a pathogen; neutral; or harmful, for example, by causing antibody dependent enhancement (ADE) or autoimmunity (*3*, *4*).

The heterogeneity in the repertoire and in the functional effects of specific antibodies can therefore determine individual susceptibility to infection or disease (*5*), but the affinity of antibodies for three-dimensional structures in their native form makes deconvoluting the polyclonal B cell response challenging (*6*, *7*). This contrasts with T cells, which inherently recognize only processed peptides derived from proteins. Antibodies typically bind multiple epitopes within each pathogen protein, such that an assay against a whole conformationally intact protein (e.g. ELISA) is an aggregate of the response and a large number of epitopes can be recognized across pathogen proteins by a population of individuals (*8*). Profiling antibody-epitope binding is therefore labour intensive and does not scale easily for most of the repertoire.

So-called “linear” B cell epitopes, those in which a continuous peptide fragment (10-20 amino acids) can bind an antibody, can be screened for using high-throughput methods thanks to their biochemical simplicity. However, these are a minor subset (~5-10%) of the whole repertoire (*7*), and most are thought to reflect functionally unhelpful antibodies that bind only degraded rather than whole proteins exposed on viable pathogens (*6*, *7*). An alternative to experimental linear epitope discovery methods are in silico tools which predict the position of discontinuous epitopes (targets of most of the antibody repertoire) within the structure of a protein (*9*). However, to date, none of these tools attempt to identify whether a minimally sufficient set of residues can recapitulate predicted epitopes.

To address this, we have developed a computationally efficient thermodynamic method for predicting which parts of a protein can form stable peptides. The idea is to identify sequences that would be most likely to adopt similar 3D conformations when synthesised as peptides compared with their context within the full-length protein. Our approach aims to enrich for peptides which we hypothesize are good candidates to be functionally relevant and immunodominant epitopes: as they are exposed on whole proteins and likely to persist in debris. Experimental efficiency is improved by 1/ not synthesizing peptides that are unstable and 2/ reducing false positives by eliminating stable peptides that will not adopt their native conformation.

We have applied this method to the SARS-CoV-2 proteome, examining all peptides between the arbitrary cutoffs of 10-100 amino acids in length, and validated the approach by characterising the antibody repertoire in independent clinical cohorts recruited within the UK National Health Service. SARS-CoV-2 is a good candidate for the discovery of beneficial and harmful targets as infection severity is variable (*10*) and antibodies are known to be both a key correlate of protection from infection (*11*) and a cause of harm (*5*, *12*). Moreover, COVID-19 outcome heterogeneity remains incompletely explained and the virus-specific factors that trigger breakdowns in tolerance and resultant immunopathology for SARS, MERS, and SARS-CoV-2 but not for other coronaviruses are not known.

Results

Validation of a computationally efficient method for predicting structurally-stable immunogenic epitopes

A 1000 amino acid long protein has 86,086 possible sub-peptides between 10 and 100 residues in length. Across the SARS-CoV-2 proteome there are 1,240,901 such peptides. As it is expensive to screen this many peptides experimentally, or computationally using complex energy functions, we took advantage of a property that is relatively simple to compute from protein structure and is directly related to the energy of protein folding: the solvent-accessible surface area (SASA). Previously, we have demonstrated the utility of SASA for prediction of protein stability, flexibility, and assembly pathways, and shown that it is competitive with much more computationally intensive structural modelling strategies (*13–15*), making it feasible here to assess a huge number of possible peptides.

Starting with all proteins from the reference SARS-CoV-2 proteome (now available at: www.uniprot.org/proteomes/UP000464024) (Fig. 1A), we selected those regions where structural models were available, and then fragmented the structures into all possible 10-100 amino acid sub-peptides. For these sub-peptides, we computed a metric we term ΔASA_r, defined as the difference in SASA between the free peptide and the peptide in the context of the full protein structure normalised by the SASA of the peptide. Peptides with low ΔASA_r make fewer contacts outside of the peptide region and are thus more likely to maintain in the free form a conformation like that in the native structure (Fig. 1B).

Importantly, this strategy was not developed to predict immunogenic regions of the proteins, per se. Although we expect of two antibody-binding peptides, the more stable peptide to be a better immunogen, all else being equal. Instead, the ‘stable’ peptides are most likely to adopt structural conformations as isolated peptides that are similar to the conformations in the full protein, and thus most likely to bind the same antibodies when expressed as peptides. Therefore, we complemented our structural method with other structural predictors of immunogenicity (see Supplemental Methods), to prioritize stable peptides from regions we judged most likely to be immunogenic and functionally relevant. For example, we prioritized peptides from the virion structural proteins, as these are the most abundant antigens. In total, we selected 100 peptides from the structural proteins (Fig. 1C), seeking to obtain broad coverage and a range of peptide sizes. The extra-virion exposed surfaces were covered in greatest depth, as these were pre-judged to be particularly likely to be functionally relevant and the Nucleoprotein was also covered in depth, as it is known to be immunodominant in SARS-CoV, where it has been described as a target of ADE-causing antibodies (*16*). We also selected 96 peptides from the non-structural proteins (Fig. 1D), again seeking broad coverage, but without prioritisation using ΔASA_r values.

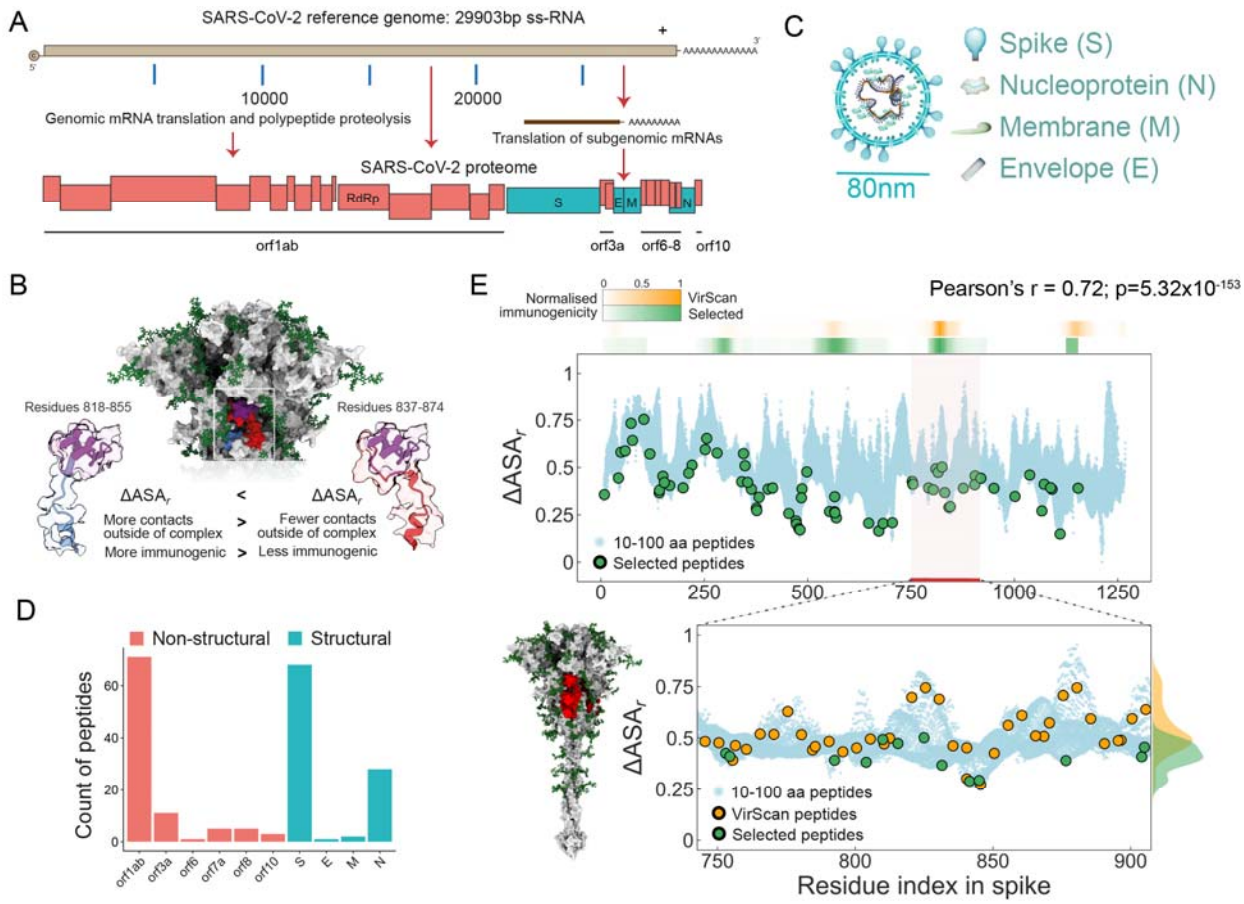

Fig. 1. Predicting structurally stable epitopes from the SARS-CoV-2 proteome. (A) SARS-CoV-2 reference genome and proteome. (Red – non-structural proteins; Cyan – structural proteins). (B) Peptides with lower ΔASA_r are more likely to adopt similar conformations as free peptides and are hypothesized to be more immunogenic than peptides covering the same region having higher ΔASA_r. (C) The structural proteins of a SARS-CoV-2 virion. (D) Count of the 196 peptides from SARS-CoV-2 proteome by viral protein. (E) Top: the blue dots show the values of ΔASA_r for all possible 10-100 residue long peptides in spike along the linear sequence. Peptides are represented by their midpoints. Green dots mark the selected peptides using our structure-guided approach. Bars on top are co-linear with the residue index and show the immunogenic profile of spike as determined by VirScan phage-display (orange) or by our approach (green). VirScan: Z-score difference, ours: ELISA ratio of positive sera to negative sera smoothened with a sliding window average of +/- 10aa and normalized to a scale of 0-1. Without using the sliding window average the Pearson's correlation is r = 0.68 ($p=8.21x10^{-129}$). Bottom: the amino acid region 750-900 of spike is shown in the structural context (left) or as a ΔASA_r distribution (right). Orange dots are midpoints of VirScan peptides, which generally have higher ΔASA_r values, as highlighted by the density diagram on the right ($p<1x10^{-3}$ comparing all Spike proteins for both methods, Wilcoxon two-sided rank sum test).

Novel expression vectors for bacterial and mammalian expression and robot-assisted cloning and recombinant protein expression and purification pipelines were designed and optimized. Using these, reliable fusion protein expression and robotic purification by affinity chromatography was

achieved: we were able to successfully purify 192/196 peptides as fusion proteins in bacteria. Isotype specific reactivities in sera were then assayed for single epitopes using indirect colorimetric ELISAs (Fig. S1).

Pooled sera (3M; Technopath, Tipperary, Ireland) from SARS-CoV-2 recovered and pre-2019 naïve subjects was used to experimentally validate the reactivity of the predicted peptides (Fig. S2). We identified reactivity across structural and non-structural proteins of SARS-CoV-2 in broad agreement with published studies using other approaches (*17*, *18*). However, we also identified reactivity where other techniques had not. For example, figure 1E, demonstrates a general overlap between our method and a phage-display method "VirScan" (Pearson's r=0.72, $p=5.23x10^{-123}$) for the Spike protein, but our method identified stronger immunogenicity at some of these regions. The VirScan library uses arbitrarily sized k-mers with arbitrarily sized overlaps which we find are often not structurally optimal, as judged by the ΔASAr criteria (Fig. 1E) (*17*). We found that by applying our structure-based approach using ΔASA_r to the VirScan data and another Phage-display-based dataset (ReScan (*18*)), we were able to predict which of a pair of overlapping peptides within these datasets spanning an immunogenic region was more immunogenic (Fig. S3). This was possible despite neither peptide in overlapping pairs being likely to be as stable as a peptide where the length and position are optimized to minimize ΔASA_r. This comprehensive external validation of our method is possible due to the intensive study of SARS-CoV-2 using data from methods that are both structure and amino acid sequence blind in their library construction. Consequently we can demonstrate unambiguously the value of the stability information in predicting immunogenicity and that this predictive capacity is not simply a function of peptide surface solvent accessibility in isolation, but is captured by the our measure of similarity between peptide and the region within the complex: ΔASA_r (Fig. S3). These analyses also show that there is scope to improve efficiency in high-throughput methods by incorporating this structural information at the outset, as these studies in general used peptides we find to be less stable than those we selected (Fig. S3).

To prioritise epitopes for characterisation with scarce individual patient samples, we ranked peptides on immunogenicity by the ratio of reactivity in pooled positive sera to pooled negative sera (Fig. 2A). Figure 2A demonstrates findings for the structural protein antigens – the spike (S), nucleoprotein (N), membrane (M), and envelope (E). Consistent with other studies (*17–19*), we found that the most immunogenic epitopes were identified within the structural proteins, particularly S and N (Fig.2B), but we also identified reactivity at the N-terminus of the Membrane protein undescribed in these studies: an extra-virion domain captured by peptide M1 (Fig.2C). After considering the positions of epitopes on the whole proteins and the immunogenicity ratios for IgG, IgA, and IgM, a subset of immunodominant non-overlapping peptides were selected for individual-level testing (Fig.2A-B). The ratio of isotype-specific immunogenicities IgM:IgG, IgM:IgA, and IgA:IgG revealed the M1 peptide in particular as an outlier. Anti-M1 IgM was absolutely and relatively higher than other antibody isotypes for M1 compared to all the other peptides (Fig.2C and Fig. S4).

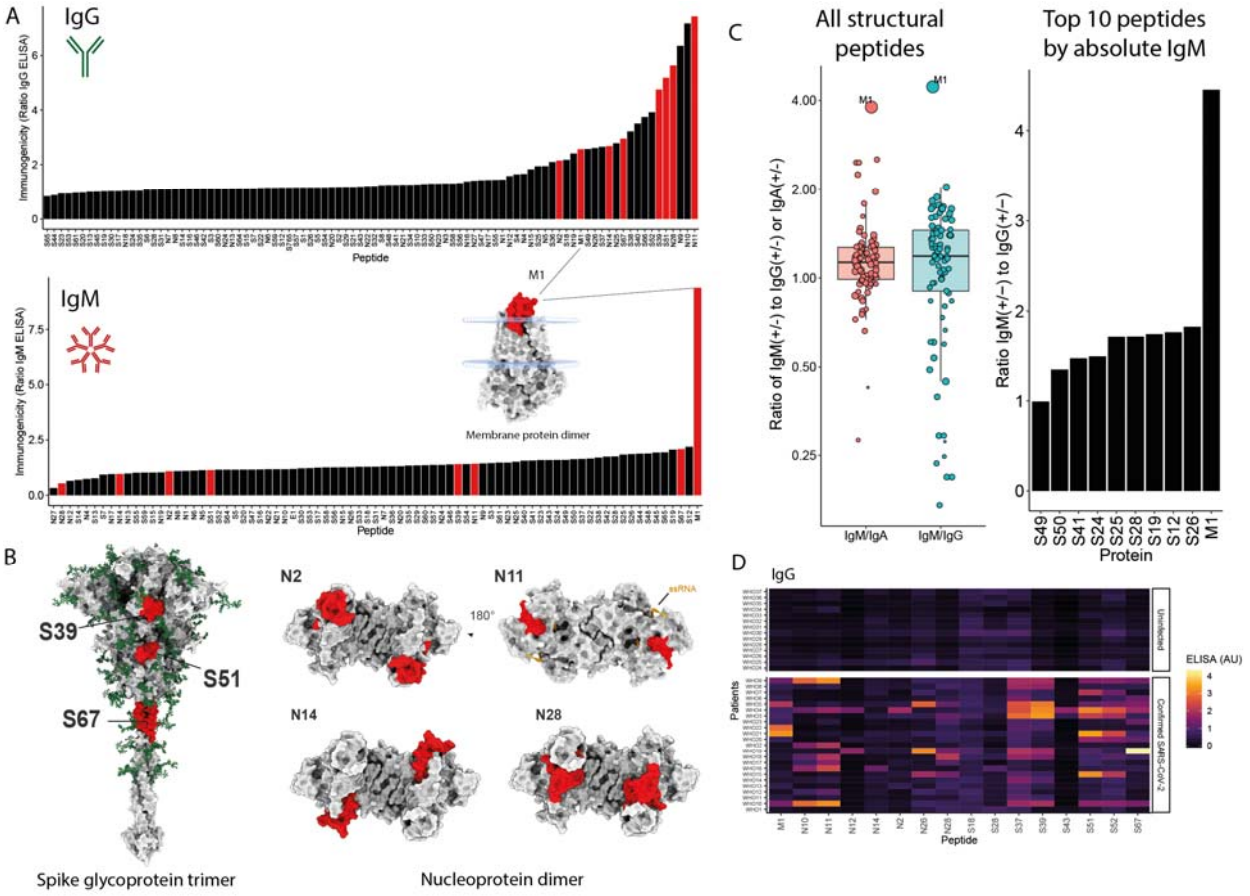

Fig. 2. Experimental validation of immunogenicity: an exposed Membrane epitope (M1) is an outlier with an IgM dominant response. (**A**) Selection (red) of eight non-overlapping peptides. Immunogenicity in bacterially expressed proteins. The ratios of the mean of at least three technical replicates for pooled positive sera to pooled negative sera (representative of at least two biological repeats (i.e. antigens expressed and purified independently) against individual peptides from the SARS-CoV-2 structural proteins. Inset shows position of the M1 epitope on the extravirion surface of the Membrane protein dimer. (B) Position of the selected (red) epitopes on the Spike trimer and Nucleoprotein dimer models. (C) Left: the ratio of IgM/IgA and IgM/IgG for all peptides. Larger size corresponds to higher IgM immunogenicity. Right: top 10 peptides selected by absolute strength of IgM response. (+/-) represents the immunogenicity ratio between SARS-CoV-2 +ve (convalescent) pooled sera and -ve (unexposed) pooled sera for the given isotype. Y axis values both panels are therefore the ratio by isotype of immunogenicity ratios. (D) Heatmap of individual NIBSC reference sera (rows) against peptides (columns) for a selection of epitopes. NIBSC reference panel uninfected individuals (top panel) and individuals after confirmed SARS-CoV-2 infection (bottom panel). Demonstrating individual heterogeneity in the immune response to the eight selected peptides and other peptides from across the structural proteins of the virus.

Antibody responses to predicted epitopes are heterogenous and public epitopes are conserved despite viral evolution and antigenic drift.

A reference set (NIBSC) of 23 individuals with PCR-verified SARS-CoV-2 and 14 individuals who were SARS-CoV-2 naïve confirmed the immunogenicity and specificity of the peptides. In contrast to the aggregate results for whole viral proteins assayed with these sera (Fig. S5), we observed substantial inter-individual heterogeneity in the response resolved to level of epitopes (Fig.2D). Nonetheless, single peptides and combinations were able to discriminate with high sensitivity and specificity between infected and naïve individuals (ROC for combination of IgG responses AUC = 0.99, Fig. S6).

We next looked at responses to these antigens in independent clinical cohorts recruited in the first pandemic wave in the UK: March-May 2020 (tables S1-6). The proportions of individuals with detectable IgG responses to each antigen was similar across the cohorts: >80% of individuals in each cohort showed IgG reactivity to at least one of the three spike peptides and >90% had reactivity to at least one of the eight epitopes across S,N, and M (Fig. S7). Surprisingly, despite SARS-CoV-2 antigenic evolution causing the emergence of variants with substantial immune escape, we found that none of the variants of interest or concern have acquired mutations in the prioritized S or N epitopes, and only the recent Omicron variants have acquired mutations within the M1 epitope. M:Q19E is common to all omicron subvariants and subvariant specific independent mutations that may impact glycosylation at the D3 position (D3G, D3N, D3Y, Fig. S7). The M:Q19E mutation has been shown to be associated with increased fitness (*20*) and it is notable that the neutral glutamine at this location found in pre-Omicron SARS-CoV-2, is shared in SARS and SARS-related bat coronaviruses, whereas acidic residues (glutamic acid or aspartic acid) are observed in most non-bat sampled coronaviruses (Fig. S8).

The extravirion M1 Membrane protein epitope response is IgM dominant, public, and predictive of correlates of protection and severity.

Given the high ratio of M1 IgM in pooled positive sera, we looked at IgM responses across a second independent cohort of 30 European individuals collected prior to 2019 to verify responses as genuine anti-SARS-CoV-2 reactivity. Consistent with findings from pooled negative sera and the NIBSC reference sera (Fig. 2D), no pre-Covid M1 cross-reactivity was observed in these samples (Fig.3A). To determine the antibody kinetics in the convalescent period, we fitted random intercept mixed effects models for isotype specific responses to individual epitopes for longitudinal follow up samples for the Edinburgh cohort (Fig. 3B). IgM titres to the M1 antigen waned quickly from high levels in the 3 months post infection for most individuals, further consistent with the IgM-dominated anti-M1 response having been provoked by SARS-CoV-2 infection.

The majority of subjects in post-COVID clinical cohorts had M1 IgM responses (Edinburgh: 71/100, Manchester: 28/36) but lacked IgG responses (Fig. 3C). The inverse was observed for the other epitopes (Fig. 3D). The IgG response to most of the epitopes was relatively stable (N28, S51) or waned significantly (N11, S39, S67) over the 1-3 months post infection. The M1 epitope was again an exception. In those individuals where M1 IgG responses could be detected, they increased significantly over the 3 months from low or undetectable initial levels (Fig. 3E and Fig. S9).

Comparison of the Edinburgh cohort (of whom few were hospitalised) to the Manchester cohort (where all the individuals were hospitalised, required supplemental oxygen, and 27/33 had bilateral chest radiograph opacification), showed a significant tendency for higher M1 IgM titre

in the hospitalised cohort (Fig. 3B). However, there are differences in the timing of recruitment and ages of subjects between these cohorts complicating interpretation of the comparison. Within the hospitalised cohort, who were recruited earliest in the course of their infection, there was an association with lower titres of IgM to M1 in older individuals (Spearman's Rho -0.63, p<.001) (Fig.3F and Fig. S10). Whereas, this was not evident in two cohorts of mildly infected individuals sampled at later time points (Fig. S10). Natural and adaptive secreted IgM are known to play important non-redundant roles in constraining viral replication early in infections (*21*), and reduced secretion of IgM is a general phenomenon reported to be associated with older age, high BMI, and male sex (*22*, *23*).

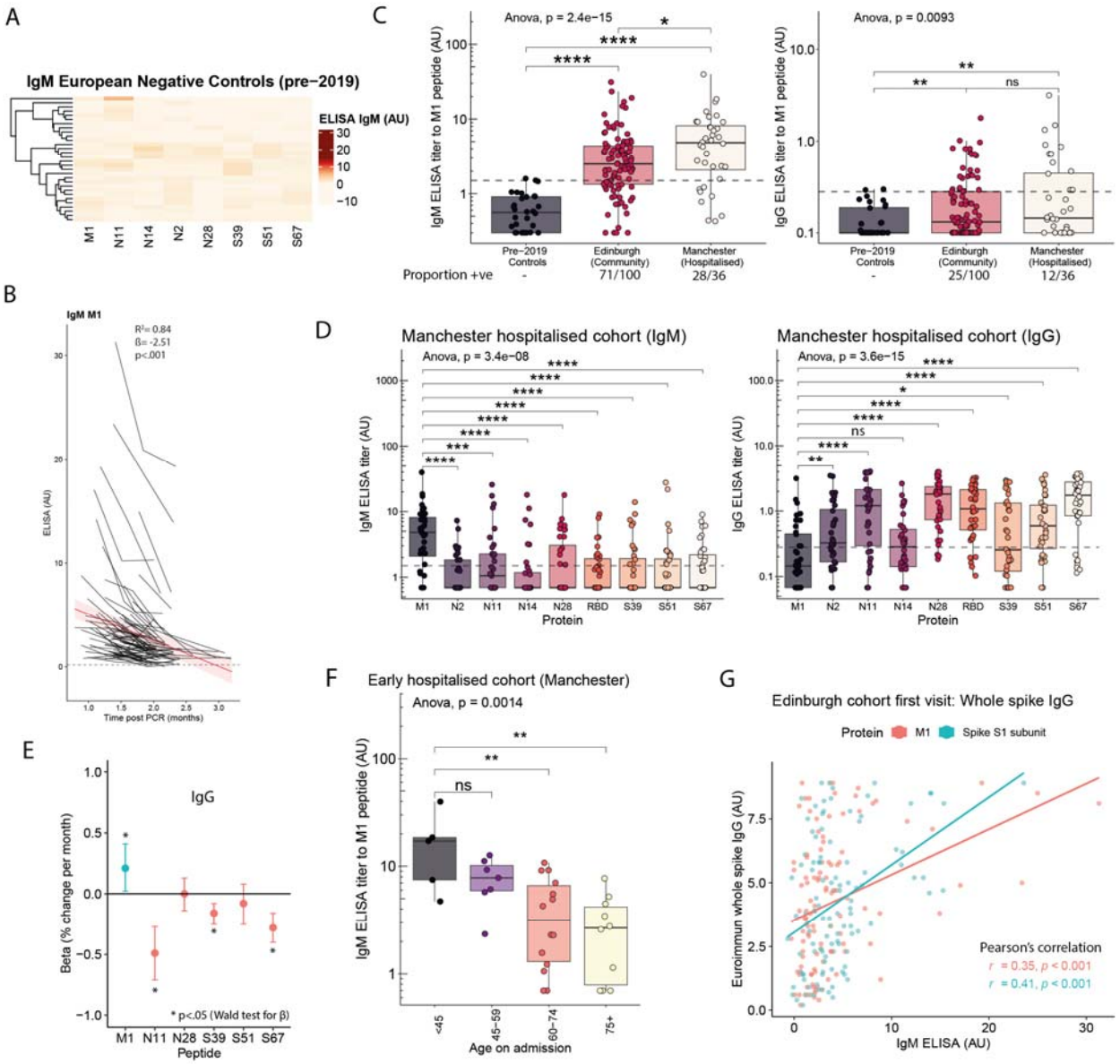

Fig. 3. The antibody kinetics for M1 antigen show it provokes a strong IgM response in most exposed persons but limited isotype class switching. (**A**) Heatmap of IgM response by ELISA for 30 European individuals collected pre-2019. (B) Proportion of three NHS clinical cohorts with M1 IgM above the mean + 3SD of the responses in A. (C) IgM and IgG titre to M1 in two clinical cohorts (Edinburgh and Manchester). Dashed line mean + 2SDs of responses for European negative controls (as in A). (D) IgM for the M1 peptide titre tends to be higher than any of the other peptides or the whole receptor binding domain early in the course of infection. (E) Coefficients for time post PCR of random intercept models by antigen. M1 is the only epitope to show a significantly increasing titre in IgG over the three months post PCR. (F) IgM titres to M1 fall over the 3 months post infection and fall fastest for those with highest titres. (G) IgM to M1 and spike S1' subunit predict aggregate whole spike IgG titre measured by a Euroimmun assay. ns = not significant, * = p<.05; ** p<.01; *** p<.001; **** p<.0001, all post-ANOVA pairwise comparisons are two-sided t-tests.

Surprisingly, M1 IgM predicted antibody responses to known correlates of immunological protection and severe disease within the Spike. M1 IgM predicted both whole Spike IgG titre by a commercial assay (Fig. 3G) and pseudovirus neutralisation titre (Fig. S12). The correlation was driven by those individuals with high IgM invariably having high total Spike antibody, but the inverse was not generally true. This observation was replicated in an independent cohort, finding that M1 IgM predicted whole Spike IgG in blood donors even 2-6 months after infection (Fig. S12). In the replication cohort the association is less strong as expected and would not be robust to correction for multiple testing if considered a discovery rather than replication cohort. Nonetheless, IgM for no other peptide (including Spike peptides) was significantly associated with whole Spike IgG, whereas IgM for the whole (multi-epitope containing) S1' subunit of the Spike was correlated with Spike IgG titres, as expected (Fig. S12). Unexpectedly, M1 IgM was of similar predictive value as IgM to the whole S1' Spike subunit, the site of most neutralising antibody binding, containing the ACE-2 receptor binding domain (*24*, *25*). Anti-RBD titres tend to be higher in individuals following severe infection but are also an important correlate of protection from infection (24).

M1 position on the virion and antibody kinetics suggest it is a T independent antigen

The membrane protein is the most abundant SARS-CoV-2 protein and forms a homodimer that binds the three other virus structural proteins (S, E and N) (*26–28*). Published analyses of virion structure show that the number of Spike trimers per virion ranges between 0 and 50 with a mean of approximately 25 pleomorphically arranged Spikes per virion, with 10-20% of virions having no spike proteins (*29*) . In contrast, on each virion approximately ~2,200 M1 epitopes are exposed on the envelope surface (Fig. 4A) (*28*). Using cryo-electron microscopy and tomography, Neuman et al. report that M dimers tend to be tightly positioned within coronavirus virions and that this organisation establishes virion shape with dimers repeating every 5^0 of radial curvature (*28*). Coronavirus membrane proteins are arranged in rhomboids with sides of approximately 4-5nm, such that the distance between membrane protein dimers across the rhomboid is approximately 7.5nm in one axis and 3.8nm in the other (Fig. 4B) (*28*). A recent modelling study of the SARS-CoV-2 envelope, suggests that M dimers may have more dynamic higher order structure and agglomerate into large filament-like repetitive macromolecular

assemblies (*30*). These studies imply that B cells with M1-binding mIg will encounter repetitive arrangements of M1 on the surface of virions without obstruction by spike proteins during infection.

In light of these studies, we hypothesized that the atypical antibody kinetics of the M1 epitope were due to it acting as a T independent B cell antigen (Fig. 4C). Antigen specific T independent (TI) B cell activation occurs in response to repetitive polysaccharide antigens or glycoproteins, and requires antigen repeats, scaffolded between 5 and 10nm apart, to recruit a local cluster (10-20) of the ~10^5 total B cell receptors on the B cell membrane to generate the necessary local signal strength (*31*). We reasoned that the abundance and repeating quaternary organization of the Membrane protein in the viral envelope, could provide this signaling in M1-specific B cells, allowing for activation in the absence of follicular T cell help (Fig. S13). This would explain the IgM dominant response we observed, as TI B cell activation is associated with extrafollicular plasmablast differentiation and the secretion of antigen specific IgM with limited isotype class switching (*31*, *32*). Isotype class switch recombination occurs predominantly in T dependent (TD) responses in germinal-center-destined B cells, where it is induced by helper T cell interaction and local cytokines at the T-cell:B-cell border of secondary lymphoid organs (*31–37*).

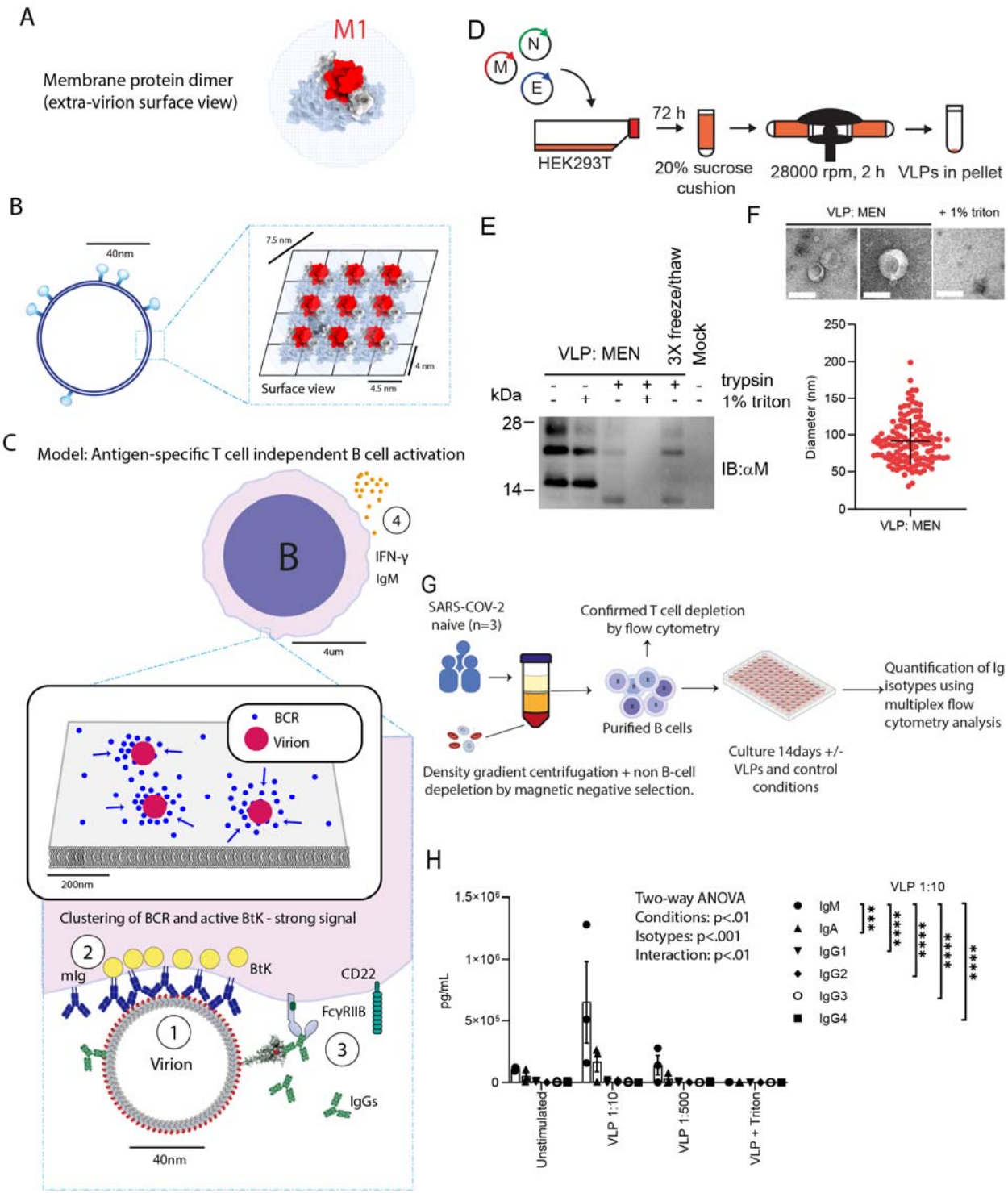

Fig. 4. Hypothesis: Lack of isotype class switching is due to T independent B cell activation triggered by the repetitive arrangement of M1 antigen on virions. (**A**) View of the membrane protein dimer from the extra-virion perspective. (B) Virions are pleomorphic in diameter and number of spikes with tightly arranged membrane proteins. (C) Model of T independent B cell activation by repetitive antigen. 1 – Virion arrangement of repeating M1 antigens engages with cognate membrane bound immunoglobulin (B cell receptors) on the surface of M1 specific B cells. 2 – secreted antibody (IgG shown) binding to surface epitopes can negatively regulate TI

responses by competing with mIg binding or by triggering signaling through surface receptors on the B cell. 3 – Cross-linking activation of 10-20 clustered B cell receptors and active BtK is sufficient to trigger calcium influx resulting in B cell activation without T cell help. 4 – Cytokine release may potentiate or be triggered by TI activation and antigen specific IgM is secreted without isotype class switching. (D) Schematic illustrating production of spikeless virus-like particles. (E) Protease protection assay: Western Blot for M protein in purified VLPs showing protease resistance in the absence of detergent. (F) Transmission Electron-Microscopy (TEM) validation of the production and expected size of spikeless VLPs. (G) Schematic illustration of in vitro B cell stimulation assay. (H) Incubation of B cells with VLPs stimulates IgM secretion compared to unstimulated (PBS) or incubation with disassembled VLPs pre-treated with Triton-X-100, which have otherwise identical protein composition. *** = adjusted p<.001; **** = adjusted p<.0001 for Tukey's post-hoc pairwise multiple comparison test. Shown are comparisons between IgM and other isotypes for VLPs at high concentration (1:10), all other pairwise comparisons were not significant.

To facilitate testing this hypothesis, we produced and purified non-infectious spike-less SARS-CoV-2 virus like particles (VLPs) in HEK-293T cells, using methods described previously (Fig. 4D) (*26*, *27*). The expression of the M, N, and E proteins is sufficient to form Spikeless VLPs in cell culture (*26*, *27*). We validated production and purification of VLPs using a protease protection assay (Fig. 4E and Fig. S14) and performed transmission electron microscopy (TEM) to confirm the expected morphology (Fig. 4F).

Next, whole blood was drawn from healthy volunteers (n=3) (Tables S7). PBMCs were extracted by density gradient centrifugation, and untouched B cells were enriched by negative selection, depleting T and other non-B cells (Fig. 4G). After culturing with VLPs/controls for 14 days, we found that B cells from 2/3 individuals had secreted IgM (Fig. 4H), consistent with our hypothesis. This was not observed in unstimulated B cells or B cells co-cultured with VLPs that had first been disassembled by detergent treatment but otherwise were expected to have identical protein composition (Fig. 4F). However, inspecting cultures before harvesting supernatant at day 14, we noted limited proliferation in this experiment. Immunoglobulin production (of all isotypes) was also much higher in positive control conditions using CpG, CD40L, and R848 (a synthetic TLR 7/8 agonist) (Fig. S15). These positive controls would be expected to non-specifically stimulate B cells, and B cells capable of recognizing M1 were presumed to be a minor subset of the total B cell repertoire, therefore in the absence of a selective proliferation of M1-specific cells we would not expect M1-specific secretory response to match non-specific B cell activation.

Reasoning that proliferative expansion of M1-specific B cells could be dependent on priming with cytokines or other factors present in the course of infection in vivo but not captured in vitro, we pursued a second experiment where we invited participants who had recently recovered from COVID breakthrough infection (n=3) (Table S7) (Fig. 5A). In this experiment, we included additional conditions where we added Il-4 (as a lymphocyte survival factor), Il-6 (characteristic of the COVID-19 cytokine storm), and the combination of Il-4 and Il-6. Mutant VLPs were also included as an improved negative control, where the constructs, culture-conditions, and purification was otherwise identical to the wild-type VLPs except where the M1 domain was replaced with the corresponding domain from the seasonal betacoronavirus OC43 (OC43-M1). We also investigated a mutant with a deleted (ΔM1) but were unable to verify these formed protease-resistant structures (Fig. S16). In addition, because the degree of TI B cell activation an

antigen provokes is known to be affected by binding competition from secreted antibodies (*31*, *34*, *37–40*), we raised and purified affinity matured and class-switched polyclonal antibodies in rabbit, using the M1 peptide as the immunogen. After validating this blocking antibody recognized conformationally intact protein (Fig. S16), as predicted by our ΔASAr method, we added this as a negative control hypothesizing that these antibodies would block a TI effect caused by M1 (Fig. 5A).

Consistent with our hypothesis, VLP-concentration dependent B cell proliferation, first visible by day 5 as discrete outgrowths of cells, was obvious in this experiment. We captured low-magnification images at day 8 and day 14 for all culture conditions. VLP-dependent proliferative outgrowths were evident in B cells from all three convalescent individuals to variable degrees in the no-added cytokine groups. Figure 5B shows the appearance of the B cell culture at day 14 for the individual P-02, the individual with the most striking proliferative response. Culture conditions are identical in all groups with the exception of the added VLPs +/- controls specified. OC43-M1 VLP exposed B cells showed little to no proliferation, and addition of the anti-M1 antibody to the VLPs before adding to B cells almost entirely abrogated the proliferative effect. The addition of cytokines, particularly the combination of Il-4 and Il-6, appeared to potentiate the VLP-dependent response for all three individuals, particularly in the individual P-01 who had the most subtle response to VLPs in the no added cytokine condition (Fig. S17). Photographs for all three individuals for all conditions and cytokines in data S4.

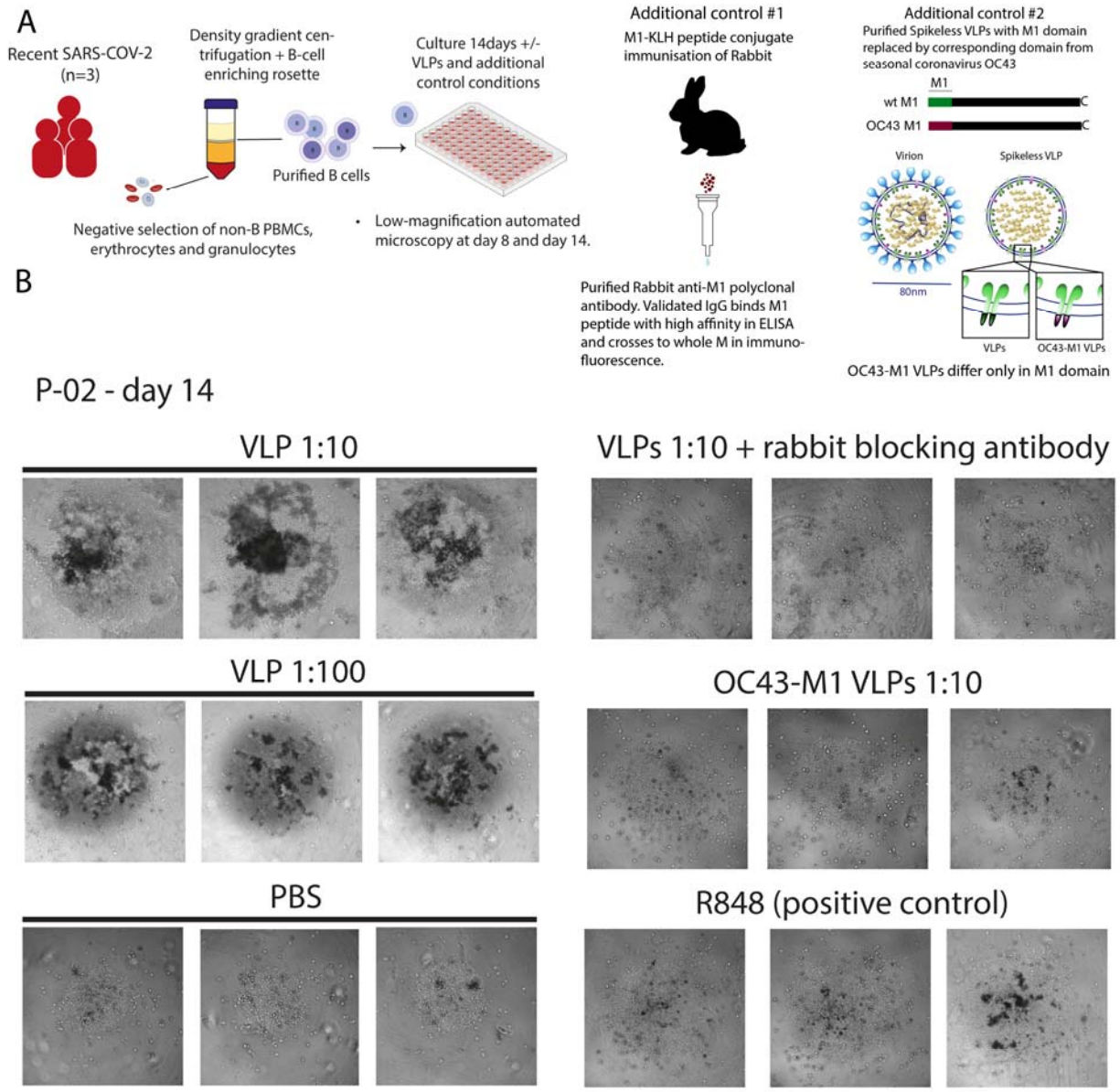

Fig. 5. Purified B cells from individuals recently recovered from COVID proliferate in response to stimulation with VLPs lacking Spike. (**A**) Experiment design schematic. (B) Data points are the mean OD of three technical replicates for each of three recently recovered individuals. Bars are means, error bars are standard error of means. Post-hoc Wilcoxon one-sided tests demonstrate a significant increase in M1 specific IgM compared to control conditions. VLP 1/10 is a high concentration VLPs, VLP 1/100 is lower concentration, PBS is an unstimulated negative control; OC43 are cells incubated with a high concentration of SARS-CoV-2 VLPs with the M1 domain replaced with the equivalent domain from the membrane protein of seasonal coronavirus OC43; and VLP 1/10 + rAb is a high concentration of wildtype VLPs pre-incubated for 15mins with a 1/500 dilution of an anti-M1 blocking polyclonal antibody raised in rabbits. R848 is a synthetic TLR7/8 agonist which non-specifically activates B cells. (C) We observed a dose-dependent proliferative effect of incubation of VLPs. Images are B cell culture technical replicates, from a single individual (P-02), who showed the most marked proliferative response taken at day 14 before harvest of supernatant for immunoglobulin quantification. Images are

from culture without the addition of cytokines, culture conditions were identical for all conditions with the exception of the added stimulant/control. Full data at both time points, for all participants and with inclusion of cytokines available in data S4.

M1 IgM is strongly associated with severe/critical COVID-19

TI responses are characterized by cytokine release from B cells and other co-activated immune cells including IFN-y, Il-6 and GM-CSF, cytokines also associated with severe COVID-19 (*31*, *41*). In addition, massive expansion of plasmablasts, absence of germinal centres, and high secreted IgM are hallmarks of critical and fatal cases of COVID-19 and result from a dominant extrafollicular response (*42–44*). We therefore hypothesized that M1 specific TI may contribute to acute SARS-CoV-2 immunopathology and that M1 IgM would therefore be associated with severe outcome as a marker of the degree of TI activation.

To address this, we investigated the IgG, IgA, and IgM antibody responses to the eight viral epitopes and to the whole receptor binding domain of the spike protein (a gift from F. Krammer) in a cohort of individuals recruited in Oxford, UK in the first wave of the pandemic, who had either been asymptomatic/mild (non-hospitalised, n=45) or who had suffered severe/critical infection (n=25). Consistent with the Edinburgh and Manchester cohorts, the majority (44/72) individuals in this cohort had detectable M1 IgM (Fig. 6A). Using Lasso penalized logistic regression including the logarithm of participant age, sex and all the isotypes for each antigen and the whole RBD, the variables with the most predictive value were ascertained. The Lasso algorithm applies an increasingly strong penalty shrinkage factor to multivariable regression coefficients such that they sequentially drop out of the model: initially improving model fit by biasing coefficients to null (the bias-variance trade off) allowing for variable selection. A high M1 IgM (defined as greater than the median value for the cohort) was the only antibody response that was a better predictor than the logarithm of age and was a stronger predictor of clinical severity than any other antibody response of any isotype including to the whole receptor binding domain (Fig. 6B). These data show that in addition to being correlated with immunological features of severe COVID, the IgM response to this epitope was strongly predictive of clinical outcome.

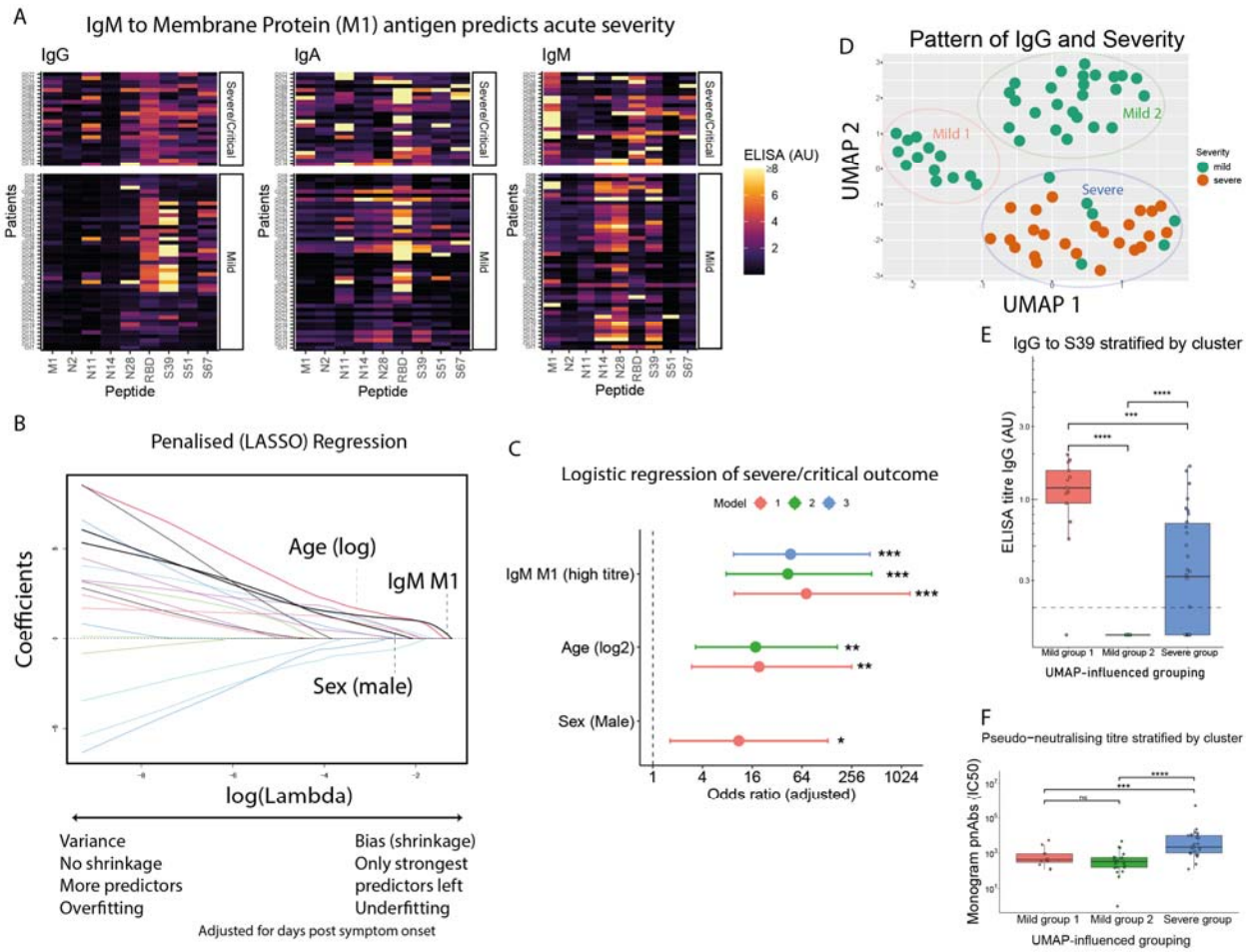

Fig. 6. M1 IgM is a strong predictor of severe/critical acute COVID-19. (**A**) Oxford cohort heatmap of individual sera (rows) against peptides (columns) for three immunoglobulin isotypes (column panels). Individuals represented by rows and separated into (row panels) by clinical severity of COVID-19 infection. (B) Penalized (Lasso) logistic regression demonstrates M1 IgM is the strongest predictor of the outcome (severe/critical COVID-19) of the ELISA responses to the eight peptides and receptor binding domain and age and sex. M1 IgM is the only antibody response that is retained in the model as a stronger predictor of severity than age. (C) Multi-variable logistic regression models (without penalisation). Points are effect size estimate (adjusted odds ratio) and whiskers 95% confidence intervals. All models adjusted for days post PCR positive. Significance indicated by * p<.05; ** p<.01; *** p<.001 for Wald test for coefficient. (D) UMAP clustering of IgG responses in (A) with colouring based on severity. (E) S39 IgG by group assigned by cluster based on the patterns in D (red = mild 1; green = mild 2; blue = severe) (F) Whole spike IgG titre (Jenner commercial assay) on Y-axis stratified by cluster pattern as in D (coloured as in E). ns = not significant, *** p<.001; **** p<.0001, pairwise comparisons are two-sided t-tests.

Consequently, multivariable logistic regression models (without shrinkage) were fitted predicting severe/critical disease on M1 IgM titre to examine the statistical relationship with other known predictors (age and male sex), and to estimate the effect size of high M1 IgM, adjusting for days post symptom onset (Fig. 6C and Table S6). These models demonstrated that having a high titre

of M1 IgM was a strong predictor of severity, independent of the effects of age and sex. The point estimate on the effect size was strikingly large: in the model adjusting for age, sex and days post symptom onset, the adjusted odds ratio for a high M1 IgM was 72.14 (95% CI: 9.71 – 1300.15) whereas the odds ratio for doubling of age (a unit increase on log2 scale) was 19.33 (95% CI: 2.96 – 256.50). The size of this effect can be emphasized by considering that high M1 IgM was associated with an equivalent odds ratio as being 75 years old versus being 20 years old. In this cohort, the model including the coefficients for days since PCR; the demographic variables of age and sex; and the single immunological parameter of M1 IgM explained a high proportion of the variation in outcome (R2 (Tjur) = 0.65). For a 60-year-old man with a high M1 IgM versus a 30-year-old woman with a low M1 IgM, the point estimate for the combined OR was >15000, albeit with wide confidence intervals.

Patterns of IgG response are also associated with severe/critical COVID-19.

Uniform manifold approximation projection (UMAP) analyses of the isotype-specific responses identified latent structure in the IgG responses (Fig. 6D) but not the IgA and IgM responses (Fig. S10). The algorithm (which is agnostic to the clinical severity and other characteristics of the participants), revealed structure, grouping severe/critical participants together based on the pattern of their IgG responses and separated the mild group into two discrete groups. We manually clustered individuals by assigning them to the three groups revealed by this approach, and found that these groupings did not so clearly associate with other potential confounders like age, sex or time since infection (Fig. S17). The severe group was characterised by high IgG to N epitopes and one S epitope (S51), and low-medium IgG titres to the S39 and S67 epitopes (Fig. 6A and Fig. S18).

Secreted antibodies that bind to repetitive TI antigens can compete with mIg binding and are known to be important negative regulators of TI B cell activation (*38*, *45*, *46*). Secreted IgG and IgM recognizing the epitope are known to be particularly important (*37*, *38*). However, secreted antibodies may also block the response even if they are not capable of directly recognizing the culprit epitope, either by steric hindrance or (in the case of IgG) through via FcR-mediated pathways (*45*). Negative regulation of TI responses occurs via inhibitory receptors that co-cluster with the B cell receptors, including CD22 and Fc gamma receptors (*31*). Signaling via these receptors in response to their binding the Fc domain of IgG bound to the M1 epitope or other co-presented epitopes (most of which are likely to be on non-neutralising regions of the Spike protein) may be important for negative regulation. These may be mechanisms by which non-neutralising IgG antibodies to any exposed structural protein epitopes (including non-neutralising Spike antibodies) could augment the severity of the immune response to infection. A striking feature of the COVID-19 pandemic has been the decoupling of efficacy of vaccinations in prevention of severe SARS-CoV-2 immunopathology, compared to prevention of infection. The reduction in prevention against infection is primarily due to the extensive antigenic escape achieved by SARS-CoV-2 viral evolution (*47*). However, the specific aspects and mechanism of the immune response that preserve protection against severe immunopathology are not well understood.

Severe patients tend to have higher anti-SARS-CoV-2 antibody titres in general (Fig. S19), and had higher neutralising titres (Fig. 6F) consistent with other studies (*27*). The S39 and S67 epitopes are of particular note in light of this, as IgG titres discriminated between the two mild groups and the highest IgG titres for these two epitopes occurred amongst group 1 mild patients,

higher than in the severe group (Fig. 6E). An IgG specific pattern would be expected of any antibodies exerting a physiologically important Fc-mediated effect.

M1 IgM persists in a subset of convalescent individuals and is associated with long COVID and symptom burden.

Given clinical recovery time post-SARS-CoV-2 infection is variable, we were interested to determine whether there were individuals for whom M1 IgM responses persisted. To explore this, we tested IgM responses in a large cohort of convalescent individuals who had donated plasma to the Scottish National Blood Transfusion service in the 2-6 months after infection against the 8 peptide antigens. A subset of individuals (22/200) showed persistent M1 IgM (Fig. 7A). K-means (k=5) clustering identified three clusters of individuals with high or medium M1 IgM, one large cluster with relatively low IgM to all the peptides, and a small cluster with IgM to S51 and N peptides (Fig. 7A).

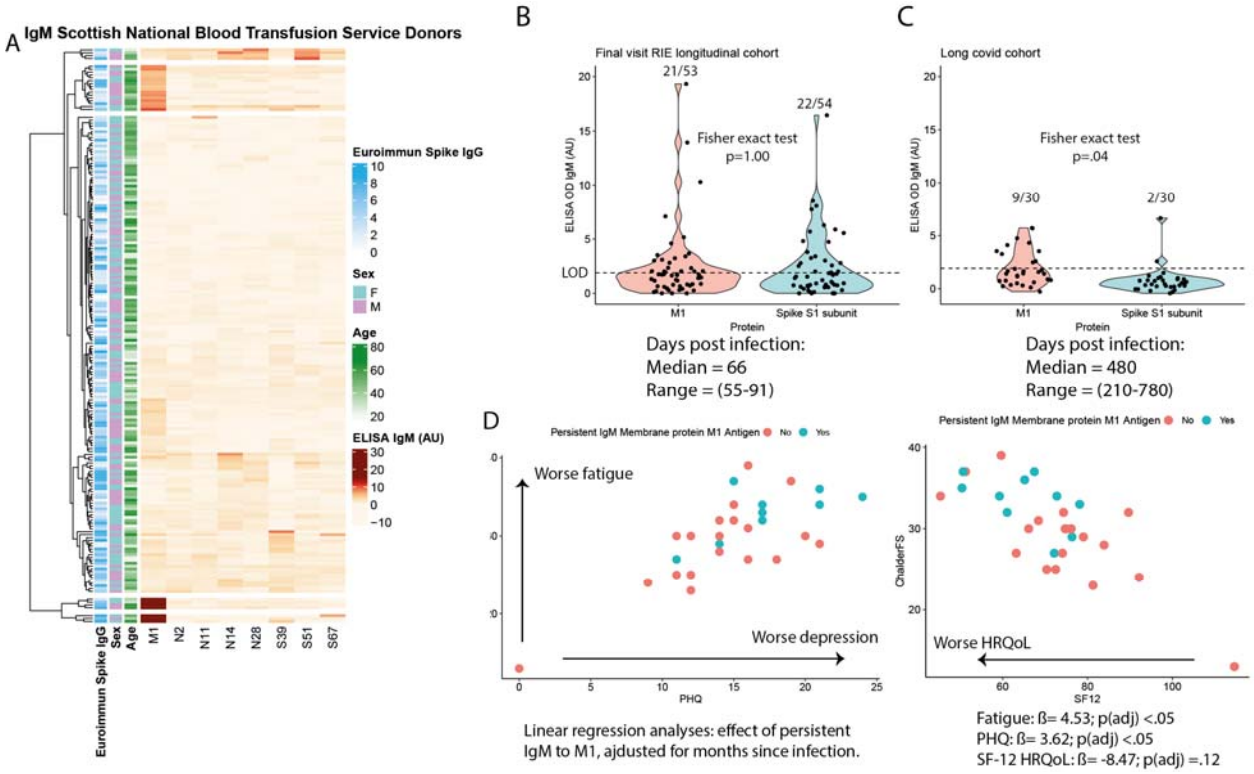

Fig. 7. Persistent M1 IgM is associated with longCOVID and symptom burden. (**A**) Heatmap of Scottish National Blood Transfusion plasma donors who donated plasma after infection early in the coronavirus pandemic for trials of therapy with convalescent plasma. K-means clustering identifies two clusters with persistent very high IgM M1 (bottom and second bottom), one cluster with little persistent IgM (large middle group), one cluster with medium IgM M1 (second top), and one cluster with persistent S51 IgM and two nucleoproteins. (B) IgM responses in the final visit of the Edinburgh cohort to M1 antigen and a whole spike S1' subunit. The whole spike S1' subunit used rather than other epitopes because no single epitope is close to the M1 epitope for IgM publicness and spike S1' subunit likely reflects an aggregate of 100s of potential epitopes. LOD = limit of detection for calling positivity based on results in negative

control subjects. (C) IgM responses in the long covid cohort to M1 antigen and a whole spike S1 subunit. (D) Chalder fatigue scale (y axis) against PHQ score for anxiety and depression. Subjects represented by points with persistent M1 IgM (cyan) and undetectable M1 IgM (red). (E) Chalder fatigue scale (y axis) against SF-12 score for a health-related quality of life score. SF-12 is comprised of two sub scores with mean 50 reflecting physical and mental domains of quality of life. Here these domains have been combined. Coloured as in D.

We next compared IgM titres to the whole spike S1' subunit and the M1 peptide in the final visit of the Edinburgh longitudinal cohort and found that 21/53 individuals were still positive for M1 IgM at a median of 66 days post infection and an almost identical proportion (22/54) individuals were still positive for IgM to the multi-epitope containing spike S1' subunit (p=1.00, Fig. 7B). However, in contrast, repeating this analysis for a cohort of 30 individuals who had been referred by a healthcare provider to a longCOVID study due to persistent cognitive symptoms (> 3 months) post infection (table S8), we found that 9/30 individuals were persistently positive for M1 IgM, whereas only 2/30 individuals were positive for IgM to the S1' subunit (p=.04, Fig. 7B). The median time since infection was substantially longer in the long COVID cohort than in any of our other cohorts (480 days). Those with persistent M1 IgM ranged from 240-780 days post infection at the time of sample draw.

In contrast to acute COVID-19, which is associated with a stereotypical clinical syndrome, long COVID is a less well-defined clinical entity where persistent symptoms are almost surely caused by a variety of mechanisms (*48*). Amongst those who have persistent symptoms will be those with permanent organ damage from the acute illness (*48–50*), and individuals with non-specific symptoms due to other physical or mental illness with onset temporally coinciding with SARS-CoV-2 infection but mechanistically unrelated. Despite the expected heterogeneity, and the small sample size, we found that persistent M1 IgM was associated with a significant 3.62 point worsening on the PHQ-15 score of anxiety and depression (p=0.048) and 4.53 point worsening on the Chalder fatigue scale (p=0.027) (Fig. 6C and Fig. S19). There was also a non-significant tendency for a worse score (-8.47) on the SF-12 health related quality of life questionnaire which combines both physical and mental domains (p=.12) (Fig. S20).

The S and N proteins of SARS-CoV-2 have been described in gut biopsies and autopsy tissues months after infection, and this has been hypothesized to contribute to persistent symptoms (*26*, *51*). As M is the most abundant viral protein and subgenomic mRNA, it is plausible that M may persist with S and N (*28*, *29*). However, to our knowledge no study has investigated the persistence of M. One prior study has investigated the severity of acute COVID-19 and the association of IgM responses to whole M and S proteins, in a cell-based assay. In that study the M protein is presumed by the authors to be presented in a similar fashion on cells as on virions. Consistent with our findings, they show membrane protein specific IgM to be associated with severe disease (*52*). However, these results would not necessarily be expected, given SARS-CoV-2 virions assemble in the endoplasmic reticulum, not at the plasma membrane (*53*).

In light of this prior work, and our findings of persistent IgM to M1 associated with longCOVID, we hypothesized that M may reach the plasma membrane in residually infected cells. Consistent with this we observe that M accumulates in islands on the plasma membrane of non-permeabilized human tissue culture cells expressing only the M protein (Fig. S21). Whether this occurs in vivo remains uncertain, but could explain the surprising persistence of IgM we detect in these longCOVID individuals, as cell surface antigen may be a more plausible mechanism for persistent B cell stimulation than the persistence of intact virions years after exposure.

Discussion

Numerous approaches exist for screening linear epitopes, however, library generation typically tiles k-mer peptides with arbitrary overlaps, so optimal biophysically stable epitope-containing peptides are usually not synthesized by chance (*17*, *19*). Which k-mers adopt similar confirmations in isolation as on the whole protein scaffold is also generally unknown. These structurally agnostic methods are of proven epidemiological value (*17*, *54*), but have low hit rates that limit downstream assays to high-throughput approaches which are not without limitations and risk missing potentially discoverable functionally important epitopes. Such systems include peptide arrays, or techniques that allow for physical linkage of the binding phenotype to genotype such as bacteriophage or yeast where epitopes are displayed on structures more than 100-fold larger than the peptides themselves (*17*, *54*). Peptides that express poorly, oligomerize these large display vehicles or aggregate with other peptides can be diminished or enriched, making quantitative interpretation challenging. Aggregation can be particularly an issue for pull-downs of multivalent antibody isotypes (e.g. divalent IgA or pentavalent IgM).

The method we describe aims to greatly improve the efficiency of functionally important epitope discovery by incorporating information about the structural stability of the peptides and conformational similarity at the outset. High yield predictions derived from experimentally confirmed or predicted protein structures can be validated experimentally in diverse downstream applications including low-, medium- or high-throughput techniques. We believe this method may have a wide range of possible applications, including in the design of peptide vaccines.

Using this approach and our synthetic-biology fusion-protein pipeline, we have identified epitopes with clinically and immunologically important correlates from the SARS-CoV-2 proteome. In particular, a non-class-switching IgM to a Membrane protein epitope. Notably, published studies profiling the antibody response to SARS-CoV-2 at the epitope level have tended to either focus on S or N, or have omitted testing IgM. Despite the vast literature on SARS-CoV-2 serology, to our knowledge, only two small studies have attempted to resolve the IgM response to specific epitopes on the SARS-CoV-2 Membrane protein (*19*, *55*), and no study has looked at clinical or immunological correlates at epitope resolution. These two studies illustrate the potential for arbitrary decisions about k-mer size and structure-agnostic tiling to impact results. Wang et al. profiled responses across the SARS-CoV-2 proteome using peptide microarrays using 15-mer and 25-mers and found IgM reactivity in only one of eight individuals for the M protein N terminus 15-mer, and no reactivity to the 25-mer peptide, which includes six additional amino-acids not included in our M1 (*19*). Our method predicted that the Wang et al 25-mer, which includes hydrophobic residues from the transmembranous region, would be the worst of these peptides (highest ΔASAr), and consistent with this prediction when tested as fusion-proteins using our pipeline we found the 25-mer to have the lowest IgM binding in ELISA from 10/10 convalescent individuals (Sup Fig. S4). In contrast, and consistent with our findings, Jörrißen et al. found a high proportion (71.9%) of 32 subjects with IgM responses to a 20-mer peptide which is similar to our M1 (19-mer), and similarly found a high IgM:IgG at two time points after infection (*55*). These data illustrate that the most immunogenic peptide is often non-obvious to structurally agnostic approaches (Figs. S2-S4).

The majority of antigen encountered in vivo by B cells is membrane bound and B cells are more efficiently activated by membrane bound antigen -- as on follicular dendritic cells or repetitive viral capsids or cell membranes -- than by antigen in soluble form (*56*). Based on the abundance and repetitive quaternary arrangement of the membrane protein within the virion, and the lack of isotype class-switching in the response, we hypothesized M1 to be a TI antigen capable of

causing extra-follicular B cell activation (*31*, *34*). Functionally important antigen-specific TI responses have been previously described for viral capsid glycoproteins including vesicular stomatitis virus (*57*)and polyoma viruses (*58*) but, to our knowledge, not for coronaviruses. Our experiments show that B cells (depleted of T and other immune cells) can be activated ex-vivo by intact VLPs lacking the Spike protein, and that recent SARS-CoV-2 infection history and cytokines influence the proliferative effects. These preliminary data support the hypothesis that the M1 IgM correlations we describe in clinical cohorts reflects a novel host:pathogen interaction. Our experiments suggest that individual factors and the cytokine context are important modifying factors but signaling via toll like receptors is also known to regulate TI responses (*59*, *60*). Further work is necessary to understand the mechanisms and contributors in detail.

A single viral antigen can potentially raise both TI and T dependent (TD) responses conditional on the circumstances of presentation (e.g. the core antigen of hepatitis B (*61*)). That we find IgM dominating the M1 antigen in response to infection, suggests that in 'natural' infection, M1 predominantly stimulates a TI response, but we hypothesized that TD responses would be provokable by peptide-conjugate vaccination. We show that the M1 peptide can be used as such a vaccine by raising high-affinity, class-switched polyclonal antibodies in rabbits that then recognize the conformationally intact full native protein (demonstrated by immunofluorescence), and we show that these antibodies block the in vitro B cell proliferative response induced by Spikeless VLPs. This demonstrates the utility of the method for identifying peptide which can also be used as immunogens to raise antibodies that recognize the conformational proteins.

That this host:pathogen interaction may be clinically significant is suggested by our findings in acute and longCOVID cohorts, but further investigation is necessary. Our study is predominantly observational, and so we are unable to discriminate causal from non-causal associations. However, the strength of the correlation and statistical independence to age- and sex- is remarkable: if high M1 IgM arose simply as a consequence of severe COVID-19, we would expect it to positively correlate with known risk factors that are themselves predictors of severe disease like age and sex. In fact, we show that M1 is anti-correlated with age in the early days after a positive test in persons who become seriously ill, and at later time points is uncorrelated. Further, it is particularly striking that high M1 IgM is observed in almost all severe cases in these cohorts. Other genetic or immunological correlates of severe COVID-19 have tended to be rare when strongly associated, or weakly associated when frequently observed, which is not the case here. For example, Bastard et al, have described rare functional auto-antibodies that neutralise 10ng/ml of both INF-α2 and IFN-ω at a 1:10 plasma dilution as associated with an OR of 67 (95% CI: 4–1109), strongly predicting severe outcome (*62*). Their findings have been replicated by independent investigators in other cohorts (*63–65*) and ours have not as-yet, and the assay and statistical approaches differ, however, notwithstanding these important caveats, it is notable that the effect sizes are similar: the adjusted OR is 72 (95% CI: 9-1300) for a high M1 IgM in our study. The pseudo-R2 for the logistic model when incorporating age and sex is strikingly high ($R^2 = 0.65$), particularly given we have not profiled some known risk factors which may account for residual variation, like anti-IFN autoantibodies. Doing so may be a direction worthy of further investigation, as patients described to have experienced severe COVID-19 with anti-interferon antibodies have tended not to have had previous severe viral infections. TI B cell activation may contribute to the breakdown of tolerance that occurs in severe COVID-19, including in individuals with other pre-existing potentially autoreactive lymphocytes, such as those antagonizing type 1 interferons.

Our findings of persistent M1 IgM in longCOVID may be a promising route for further study. LongCOVID is undoubtedly mechanistically heterogenous, and biomarkers are urgently needed to help stratify patients and to objectively score the outcome of trials of therapy and to track the natural history. The cut-off threshold used to determine IgM persistence here was stringent, and the sensitivity of the assay can almost surely be improved as we optimized our ELISAs for detection in the immediate convalescence period. Further work may therefore focus on increasing sensitivity and quantification, as persistence was significantly associated with fatigue and anxiety/depression, symptoms which place a large burden on quality of life (*48*, *50*, *66*). The biology of fatigue in autoimmune and post-viral conditions is poorly understood, despite the importance of this symptom to patients. Identifying an immunological correlate is therefore encouraging. Similar approaches interrogating the role of B cell activation and IgM may be warranted in other post-viral fatigue and autoimmune syndromes. However, in our opinion these preliminary results should be interpreted cautiously, even if they are replicated elsewhere. Many of the participants in the long COVID cohort had identifiable and treatable clinical syndromes contributing to their symptom burden (e.g. depression and migraine) and whilst our results may be consistent with an immunological perturbance – immunological mechanisms have been hypothesized to underlie the aetiology of many such syndromes – more work will be necessary to determine the possible clinical significance.

The lack of mutations in the S and N peptides, despite extensive adaptive evolution and antigenic escape to date, would be consistent with either these epitopes not being under selective pressures or the virus paying a high fitness penalty for mutations in these structurally stable domains. Severe COVID-19 is a late event in the course of infection, whereas most transmission occurs early (*67*), and so a lack of selective pressure would not necessarily rule out a role for these epitopes determining disease severity. The exception to the conservation across variants is in M1 where mutations have arisen in the Omicron variants (Fig. S6). The M protein of coronaviruses is a well-studied model of N- and O-linked glycosylation and strain-specific variation in M glycosylation is thought to determine organ-specific tropism and pathogenicity of murine hepatitis coronavirus by incompletely understood mechanisms (*68–70*). BA.5 has an D3N mutation which may be associated with novel N-glycosylation, and there are now at least three polymorphisms circulating in the Omicron subvariants at this position. A large M1 insertion has also been described in a cryptic lineage from a chronically infected individual (*71*), and recent animal work has suggested that the change in disease severity associated with Omicron is not explained by Spike mutations (*72*). M1 mutations may therefore be worth investigating directly for intrinsic differences in disease phenotype or immunogenicity of emerging variants.

The mechanistic triggers that lead SARS-CoV-2, and only certain other coronaviruses, to provoke an immunopathology characterised by massive B cell/plasmablast extrafollicular expansion, and IgM and cytokine secretion are unknown. The cytokine and immunological response associated with TI antigens is known to overlap the biomarkers of COVID-19 specific immunopathology observed in large cohort studies (particularly high IFN-gamma, GM-CSF, soluble IgM and increases in plasmablasts) (*31*, *42–44*, *73–75*). TI activation of B cells creates expansion of B cells without the oversight of T follicular regulatory cells, and this could explain why SARS-CoV-2, more than other viruses is associated with breakdowns in immune tolerance, and tissue-specific and temporal uncoupling of inflammation from viral load (*76–78*). Co-clustering of negative regulators, like CD22 and FcγR with the BCR, provides an actionable mechanism by which non-neutralising IgG binding on the virion to conserved targets (e.g. on S or M) may downregulate immunopathology contributing to the striking decoupling of protection from infection and protection from severity observed after vaccination despite extensive viral

antigenic evolution at the sites of neutralising antibody binding (*31*, *38*). Finally, the N termini of SARS and SARS-CoV-2 membrane proteins show high homology, suggesting that this mechanism may be relevant to other coronaviruses which cause immunopathology. A clear line of sight to therapeutic or preventative intervention would exist if blocking the TI response reduces severity of pathology or inhibits viral replication.

Methods

Computational prediction of thermodynamically stable immunogenic peptides

We define ΔASA as the difference between the solvent-accessible surface area (SASA) of the peptide in isolation and the peptide in the context of the full complex, if available, otherwise the monomeric structure is taken. The ΔASA is directly related to the free-energy of hydration of the peptide. To derive ΔASAr, the difference is normalised by the SASA of the peptide:

$$\Delta ASA_r = (SASA_peptide - SASA_full)/SASA_peptide$$

Thus, ΔASAr is a value between 0 and 1, expressing the magnitude to which native contacts of the peptide residues are made with residues outside of the peptide region, rather than being made within the peptide itself. Therefore, a peptide with a lower ΔASAr is more likely to adopt a conformation similar to that in the native structure, which is, intuitively, an important quality of B cell antigens.

For all the peptides occurring in the joint set of SARS-CoV-2 proteins, we generated a peptide-level structural data set by searching the Protein Data Bank (PDB) for SARS-CoV-2 structures from the original "Wuhan" sequence now available at [https://www.uniprot.org/proteomes/UP000464024], as well as closely related structures from SARS-CoV-1 with at least 90% sequence identity to the SARS-CoV-2 proteins. We also included homology models that were available at the time. These include the I-TASSER predicted nucleoprotein model (QHD43423.pdb) made available by the Zhang Lab at https://zhanggroup.org/COVID-19/; the AlphaFold predicted membrane protein monomer modelled as a dimer by the Feig Computational Biophysics Lab, which was made available at https://github.com/feiglab/sars-cov-2-proteins/blob/master/Membrane/M_dimer_new.pdb; and a model of the pentameric envelope protein, which was generated in-house. Briefly, the sequence was submitted to Phyre2 (*79*) on intensive mode on 25/03/2020, followed by sequential alignment in PyMOL to the structure of the SARS-CoV-1 E protein (5x29) and symmetric refinement using GalaxyRefineComplex (*80*).

We calculated the SASA of each peptide in isolation (i.e. without other atoms in the structure file), and in the context of the full complex or the monomeric structure. The SASA was calculated with the software AREAIMOL from the CCP4 suite (*81*), using the default surface probe radius of 1.4. We further limited the data to peptides without missing residues in the structures, and when peptides mapped to multiple structures, we selected the one with the highest resolution.

To generate an initial set of epitope candidates, we ran a wide selection of sequence- and structure-based epitope prediction methodologies to produce linear and discontinuous epitopes for SARS-CoV-2 proteins: BepiPred (*82*), SEPPA (*83*), Discotope (*9*), EPSVR(*84*), and BEpro

(also known as PEPITO) (*85*). We also generated a 10-member structural ensemble of the available homology models with the CABS-flex software (*86*), and ran ElliPro (*87*) on each member of the conformational ensemble. This step increases the number of linear epitopes ElliPro can detect, because surface regions have different SASA profiles across the conformers. Then, we searched within immunogenic regions for peptides that have low ΔASAr values. The top scoring peptides for structural proteins were visually inspected in PyMol, resulting in 100 peptide candidates. Peptides for non-structural proteins were selected based on the outputs of the above linear and discontinuous epitope predictors. Initial screening found these to be less commonly B cell epitopes and consequently we focused on Structural epitopes for our studies with limited patient material.

External validation using publicly available Phage-immunoprecipitation data

To test the utility of the ΔASAr parameter for the prediction of immunogenic peptides, we made use of publically available peptide-tiling experiments with associated immunogenicity scores. Two such data sets were available at the time of our screening experiments (after we had established our synthetic biology pipeline; these were not available at the time that we selected our prioritized peptides), which will be further referred to as VirScan (*17*) and ReScan (*18*). VirScan employed 56 and 20 amino acid (aa) long peptides, while ReScan used 36 aa long peptides in a phage display setting to identify those most enriched for binding to immunoglobulins extracted from human patient sera. In case of the VirScan peptides, we downloaded Table S4 provided by Shrock et al., 2020, and averaged over the IgG Z-scores for all positive and negative cases and took the difference as the immunogenicity signal. In case of the ReScan data, we downloaded the data files from https://github.com/UCSF-Wilson-Lab/sars-cov-2_ReScan_VirScan_complete_analysis, then extracted all SARS-CoV-2 specific peptides' read counts from the pancorona folder, excluding healthy patient sera and controls. Subsequently, for each peptide we calculated the mean read count, filtered for a minimum of 50 reads, and took these values as the immunogenicity signal.

We then asked whether lower ΔASAr values are associated with a higher immunogenicity signal. To assess this, we leveraged the adjacency of the peptide tiles, i.e. the fact that they overlap and thus cover a large fraction of the same potentially immunogenic region. In the ReScan data, the overlap is exactly 50%, while in the VirScan data 20-mer tiles have a distance of 5 aa between their midpoints (75% coverage), and 56-mer peptides have 28 aa between their midpoints (50% coverage). We calculated in any given peptide pair the number of times the peptide with the lower ΔASAr is the one with the higher immunogenicity score. We show this analysis in Figure S3A with results pooled for 56-mer and 20-mer peptides, filtered at different Z-score cutoffs. The results suggested that the hypothesized relationship holds in the large majority of cases when we only consider peptide pairs covering the most immunogenic regions (16 out of 20 pairs, $p = 5.9 \times 10\text{-}3$, binomial test). To approach the problem from a different angle, we binned members of adjacent peptide pairs in the ReScan data set according to "lower" and "higher" ΔASAr values, and compared the distribution of mean read counts between the two bins. This analysis revealed that the peptides with lower ΔASAr have a significantly higher immunogenicity signal than their adjacent partners with higher ΔASAr values (228 pairs, $p = 8.6 \times 10\text{-}3$, Wilcoxon signed-rank test). Furthermore, the trend does not hold to a significant extent when the SASA of the peptide (ASApeptide) or the relative accessible surface area of the peptide (RASApeptide), calculated as the ratio of the observed SASA to the sum of the residues' theoretical maximum, is considered, suggesting that the origin of the trend is not simply that immunogenic regions tend to

be more exposed to solvent. These analyses demonstrate that this simple structural measure, ΔASAr, is useful for the prioritisation of computationally generated peptides for laboratory-based immunological screening experiments.

Protein model visualisations

Structures of SARS-CoV-2 proteins for visualisation in figures were produced as follows. The Feig lab Membrane protein model was used to create a membrane immersed form of the dimer on the PPM 3.0 server (*88*). The fully glycosylated spike protein was acquired from the CHARMM-GUI Archive in the open and closed conformations (6VSB 1_1_1 and 6VXX 1_1_1), which are freely available at https://www.charmm-gui.org/?doc=archive&lib=covid19. The nucleoprotein dimer was generated in-house using a homology modelling approach. A scaffold structure was generated by submission of the full length N-protein sequence to Phyre2 (*79*) on intensive mode on 02/04/2020. The N and C-terminal domains were replaced with the corresponding regions of 6m3m chain A and 2gib chain A, respectively, and a homodimer was created by structural alignment to the 2gib biounit in PyMol. The structure was subsequently refined with the software GalaxyRefineComplex (*80*) using a C2 symmetric refinement protocol. For visualisation in figures, a 10-mer ssRNA was transplanted from the structure 7act. Figures were prepared with UCSF ChimeraX v1.3 (*89*), PyMol (v2.4.0, Schrodinger, LLC), and Adobe Illustrator (2022).

Synthetic biology peptide-fusion protein pipeline

Vector construction

After identification of putative immunogenic peptides, DNA sequences were designed corresponding to the fragments flanked with recognition sites for the type IIS restriction enzyme BsaI. A second, unique restriction site was also included for diagnostic purposes. These were synthesised by a commercial manufacturer (IDT) in the form of eBlocks Unique overhangs, generated by BsaI digest, at the 5’ and 3’ ends of the DNA fragments allowed the directional insertion into expression vectors using Golden Gate cloning. New vectors were made (i) for expression in mammalian cells and (ii) for expression in bacterial cells, and designed to include useful characteristics to enable stable, high level protein expression. For both mammalian and bacterial vectors a similar design framework was used so that DNA libraries could be efficiently ligated into both vectors using a high-throughput robotic platform. The general outlayof the vectors consists of the following components: a host-specific promoter, histidine purification tag, protease cleavage site, fusion protein domain, afragment with two BsaI directional cloning sites, and a termination/polyadenylation site (Fig S1). The bacterial construct uses an inducible T7-LacO promoter and contains a LacI gene in its backbone. To anchor the small, SARS-CoV2 derived peptides it has a GST fusion protein domain, whilst the mammalian construct uses a rabbit Fc fusion domain. The mammalian vector also contains an IL2 leader sequence for secretion in the culture media. Design considerations and experimental testing of the various vector components to identify those with the best and most consistent protein expression will be described in detail elsewhere. DNA libraries were cloned into the vectors as described; individual clones were confirmed by diagnostic restriction enzyme digest and verified by Sanger sequencing.

Bacterial protein expression and robotic affinity chromatography protein purification

35ul of T7 Express E. coli competent cells (NEB) were heat-shock transformed with ~25ng of plasmid DNA and outgrown in 200ul SOC media for an hour at 37^0c in 1.5ml Eppendorf tubes shaking at 500rpm on a benchtop heated shaker. 100ul of outgrowth was then added to 4ml Luria-Bertani (LB) media with 100ug/ml ampicillin in 24 deep-well plates, covered with aeraseal and grown overnight at 250rpm, 37^0C, until late log phase. The following morning these were subcultured and grown to an OD of 0.4-0.6, shifted to 18^0C and IPTG was added to 0.5 mM. After overnight expression, the bacteria were pelleted by centrifugation at 4000G, media was discarded and pellets washed in PBS. The pellets were kept frozen at -20^0C until purification.

E. coli pellets were resuspended in 500ul of BugBuster (Millipore, 70584) buffer with 1ul of 400x PMSF and 1ul of Benzonase in the 24 well plates. Resuspended samples were shaken for 30mins at 250rpm in 25^0C incubator for lysis then centrifuged at 4000G at 4^0C with this temperature maintained for all subsequent steps. The supernatant of each lysate from four 24 well plates was transferred to a 96 deep well plate for purification in a Kingfisher Flex robot (Thermo Fisher) using a custom program. Samples were added to 100ul Pierce Nickel-NTA magnetic agarose bead suspension (ThermoFisher, 78605) 25ul settled bead volume, after beads were equilibrated in (50mM sodium phosphate, 0.3M NaCl, 0.05% Tween 20, pH 8.0) with 15mM freshly prepared imidazole. After binding samples with mixing for 1 hour, protein-bound beads were magnetically collected and were washed twice in the same buffer with 30mM imidazole. Proteins were then eluted in two fractions from the beads in 100ul of elution buffer (detergent free base buffer with 500mM imidazole). Eluted proteins were immediately desalted using Sephadex columns (PD Multitrap G-25, Cytivia, 28918006) into storage buffer (PBS with 10% glycerol).

Mammalian protein expression

Expi293 cells were transfected in 6-well flat-bottom plates using expifectamine transfection kit as per manufacturers recommendations and were grown at 37^0C in 8% CO2 in expression media on an orbital shaker at 100 RPM. Supernatant was harvested at day five and kept at -20^0C until purification. The mammalian protein was purified by adding the supernatant directly to 100 ul of magnetic beads. Beads were washed with 1ml base buffer and eluted in 100ul elution buffer. Samples were desalted using Sephadex columns (PD-10 MiniTrap Sepahdex G-25) into storage buffer.

SDS-PAGE electrophoresis

Purified fusion-protein samples were prepared for gel electrophoresis with Laemelli loading buffer (final conc. 31.5mM Tris-HCL, pH 6.8, 10% glycerol, 1% SDS, 0.005% Bromophenol Blue) with 100uM dithiothreitol and heated for 5 mins at 90^0C, and were run out on SDS-PAGE gels (4-12% Bis-His in MOPS buffer). Gels were washed in warm distilled water three times to remove SDS and stained for one hour after being heated once in a microwave with 0.2% w/v Coomassie Brilliant Blue G250 in 0.1M citric acid and then de-stained in distilled water overnight before photographing.

Protein Quantification

Protein quantification was performed after desalting samples as described above, as comparison of the reproducibility of various protein quantification methods found all to be unreliable in the presence of imidazole at either 300mM or 500mM. NanoOrange (Invitrogen, N6666) showed acceptably low protein-protein variability and was practical for high throughput quantification using manufacturers protocol. Proteins were quantified at a 10x dilution for

mammalian expressed proteins and 200x dilution for bacterial expressed proteins. Duplicates were read in 96-well black OptiPlates at ~485/590nm.

Experimental validation of immunogenicity

Subjects

In total 605 serum samples were analysed for 454 individuals who had been infected with SARS-CoV-2 and 50 samples from 50 individuals collected prior to 2019. All subjects were recruited following protocols approved by local ethics committees. Informed consent was collected following committee recommendations in all cases. Further processing of patient samples and deidentified personal data was performed according to procedures, risk assessments and protocols under over-arching ethical approval from the Edinburgh Medical School Research Ethics Committee of the University of Edinburgh (reference: 21-EMREC-010). Local ethical approvals and cohort recruitment details for sample collection are detailed under cohort descriptions below.

Serum samples for assay development

Peripheral blood samples (serum and plasm) for assay development were obtained after informed consent from volunteers at University of Edinburgh. These were centrifuged immediately after collection and aliquoted. Aliquots of plasma/serum samples were heat-inactivated (56^0C for 1h) and stored at 4^0C until use.

Technopath pooled and NIBSC reference sera

CE-marked anti-SARS-CoV-2 verification panel of 37 samples was used in ELISAs for confirmation of epitope immunogenicity. Samples contain human plasma and Bronidox at 0.05% (w/vol) as a bacterial growth inhibitor. 23 samples were from known anti-SARS-CoV-2 positive individuals (WHO1-23 in this study) and the remaining 14 reported as SARS-CoV-2 naïve individuals (WHO24-37). No clinical information was available beyond infection status for these samples. Laboratory values were provided for results of commercial antibody tests (Fig. S4).

Manchester

Ethics: Cohort ethical approval was obtained from the National Research Ethics Service (REC reference 15/NW/0409 for ManARTS and 18/WA/0368 for NCARC).

Subjects were recruited from Manchester University Foundation Trust (MFT), Salford Royal NHS Foundation Trust (SRFT) and Pennine Acute NHS Trust (PAT) under the framework of the Manchester Allergy, Respiratory and Thoracic Surgery (ManARTS) Biobank (study no M2020-88) for MFT or the Northern Care Alliance Research Collection (NCARC) tissue biobank (study no NCA-009). Informed consent was obtained from each patient, clinical information was extracted from written/electronic medical records including demographic data, presenting symptoms, comorbidities, radiographic findings, vital signs, and laboratory data. Patients were included if they tested positive for SARS-CoV-2 by reverse-transcriptase–polymerase-chain-reaction (RT-PCR) on nasopharyngeal/oropharyngeal swabs or sputum during their in-patient admission for COVID-19. Patients with negative nasopharyngeal RTPCR results were also included if there was a high clinical suspicion of COVID-19, the radiological findings supported the diagnosis, and there was no other explanation for symptoms.

Samples (100ul serum) on dry ice and de-identified subject data were transferred to the corresponding authors under a material transfer agreement between the University of Manchester and the University of Edinburgh.

Edinburgh cohort

Ethics: Cohort samples were obtained under ethical approval granted through the NHS Lothian BioResource (SR1407) and London-Brent Research Ethics Committee (20/HRA/3764 IRAS:28653). All participants gave written and informed consent for serial blood sample collection.

Samples (300ul serum) and deidentified subject data were transferred to the corresponding authors internally withing University of Edinburgh without material transfer agreement.

Oxford cohort

Ethics: Severe/critical samples were collected under Sepsis Immunomics project (Oxford REC C, reference:19/SC/0296) or ISARIC/WHO Clinical Characterization Protocol for Severe Emerging Infections (Oxford REC C, reference 13/SC/0149) or consenting into the CMORE study protocol (Northwest–Preston REC, reference 20/NW/0235). Asymptomatic/mild samples were collected under the Gastro-intestinal Biobank Study in Oxford: 16/YH/0247, approved by the research ethics committee (REC) at Yorkshire & The Humber - Sheffield Research Ethics Committee on 29 July 2016, which has been amended for the purpose of the COVID-19 substudy on 8 June 2020.

Severe/critically ill patients were recruited from the John Radcliffe Hospital in Oxford, UK, between March and May 2020 by identification of patients hospitalised during the SARS-CoV-2 pandemic. Time between onset of symptoms and sampling was obtained for all patients. Written informed consent was obtained from all patients. All patients were confirmed to have tested positive for SARS-CoV-2 using the reverse transcriptase polymerase chain reaction (RT-PCR) from an upper respiratory tract (nose/throat) swab tested in accredited laboratories. The mild/asymptomatic group were predominantly healthcare workers recruited from Oxford University Hospitals NHS Foundation Trust after a positive SARS-CoV-2 PCR test in April-May 2020.

Blood samples were collected and separated into plasma by centrifugation at 500 g for 10 mins. Plasma was removed from the uppermost layer and stored at −80°C. Samples (60-150ul plasma) on dry ice and deidentified subject data were transferred to the corresponding authors under a material transfer agreement between the University of Oxford and the University of Edinburgh.

Scottish National Blood Transfusion Service (SNBTS) cohort

Ethics: Use of samples for this study were approved by the SNBTS Research and Sample Governance Committee (reference: SG2021-25).

Scottish blood donors provided informed consent for microbiological testing at their donations under SNBTS Blood Establishment authorization. Samples were collected between 01/10/20 and 21/03/21.

Long COVID cohort

Ethics: The long COVID study was approved by North of Scotland Research Ethics Committee ref 21/NS/0035.

The long COVID samples were taken from consecutive participants in a cross-sectional prospective cohort study of adult patients with persistent cognitive symptoms that lasted for greater than 3 months after COVID-19 in Edinburgh, UK, referred by hospital clinicians or general partitioners, Patients were reviewed at the Anne Rowling Centre for Regenerative Neurology at the Royal Infirmary of Edinburgh by consultant neuropsychiatrists for detailed clinical phenotyping and plasma was taken at time of consultation. Samples and deidentified subject data were transferred to the corresponding authors internally within University of Edinburgh without material transfer agreement.

Indirect ELISA

Flat-well, Greiner Microlon-coated high protein binding 96-well ELISA plates wells were coated in duplicate with 50ul of 1.25ug/ml of recombinant protein suspended in coating buffer (15mM Na2CO3, 35mM NaHCO3, pH 9.3-9.6) and incubated at 4^0C in a stationary humidified container overnight. After binding, the plates were washed four times with PBS-T (1.9mM NaH2PO4, 8.1mM Na2HPO4, 150mM NaCl, pH 7.2-7.4 + 0.05% Tween-20). Plates were then blocked with blocking buffer (1% skimmed milk powder in PBS-T) for 90 minutes at 37^0C. After washing, serum samples were diluted 1/50 in blocking buffer before 50ul was added to the desired wells for 90 minutes at 37^0C. Plates were washed again as before and secondary antibody in blocking buffer was added: rabbit anti-human horse raddish peroxidase anti-IgG (1/3000), -IgA (1/500), or -IgM (1/500) (Dako, Agilent Technologies Denmark). After an hour of incubation, plates were washed and bound secondary antibodies were visualised by adding 100ul per well of 0.04mg/ml O-phenylenediamine dichloride (OPD, Sigma) and 0.012% hydrogen peroxide in development buffer (24.5mM citric acid monohydrate, 52mM Na2HPO4, pH 5.0). The reaction was quenched using 2M H_2SO_4 based on A450nm of 0.7-0.9 and optical density (OD) at 492nm. The reaction-quenched plates was then read and recorded on a Labsystems Multiskan Ascent plate reader, plates were photographed, and data imported for analysis using R. Preliminary experiments were performed with dilutions of pooled and individual sera to determine the optimum antigen (1.25ug/ml) and serum (1/50) concentration for the assays. Sample data points were excluded only where during ELISA a pipetting error occurred and was noted, or if controls on the plate were not satisfactory the whole plate was repeated. Samples were used up in the testing of samples and so antigens were prioritized based on limited samples and some samples were exhausted before all antigens could be tested.

ELISA analysis

ELISA results were corrected based on the blank controls on each plate and normalized to a positive plate control. The ratio of the sample reading to the positive plate control reading allowed for quantitative interpretation of antibody titre at a single dilution sparing clinical samples. All ELISA “titres” referred to in this study are these adjusted ratios and are expressed in arbitrary units (AU). Dilution experiments with abundant pooled and negative sera ensured that the antigen concentration and serum dilution was in the linear range for all of the epitopes. This was achievable as only one or a small number of epitopes are expected for each peptide and peptides are attached to the same large fusion protein reducing protein-protein variability in quantification. Replication experiments performed by different study investigators on different days ensured the methods gave consistent results. Samples were assayed in triplicate or in

duplicate when serum sample scarcity required. The investigator performing the ELISAs was blinded to the clinical status and participant characteristics for all samples.

Ratio of antibody responses used to rank epitope immunogenicity are mean of 3 titre results from pooled positive samples/mean of 3 titre results for pooled negative samples. Positive and negative pools were run simultaneously on the same plates at the same dilutions of primary and secondary antibodies and antigen. Arbitrary interpretation of these immunogenicity ratios is as follows: Positive (Ratio >=1.5), Negative (Ratio <1.2), Borderline (1.2=<Ratio<1.5).

For binary (positive/negative) interpretation of ELISA assays, we took a mean of blank corrected technical replicate ODs before dividing by the mean of positive plate control (whole spike S1' subunit and pooled positive sera 1/50 dilution). The cut-off for positivity for each antigen was determined for each secondary antibody by the plate-corrected mean of negative controls + 3 standard deviations.

Pseudovirus neutralization assays

Pseudovirus neutralization experiments have been previously described for both the Edinburgh cohort and the Oxford cohort. These data were used in the analyses described in this paper (Fig. 5F and Fig. S9).

The Edinburgh cohort pseudovirus experiments/results have been previously described in detail (*90*). A brief summary of those method is as follows: 5x serially diluted serum from convalescent individuals were incubated with SARS-CoV-2 pseudotyped virus for 1 h at 37 °C. The mixture was subsequently added to 293TAce2 cl22 cells at a starting serum dilution of 1:50. Nanoluc Luciferase activity in lysates was measured 48 hours post-inoculation using the Nano-Glo Luciferase Assay System (Promega) with the Glomax Navigator (Promega). Relative luminescence units were normalized to those derived from cells infected with SARS-CoV-2 pseudotyped virus in the absence of serum. NT50 are half-maximal neutralization titers for sera determined by four-parameter nonlinear regression (GraphPad Prism).

Analysis of experimental results

Linear mixed effects regression analyses of Edinburgh longitudinal samples

We fitted linear mixed-effects models (estimated using restricted maximum likelihood) for IgM and IgG antibodies on each protein including a random intercept for the participant. For fitting the models we included only participants who had at least one detectable antibody response of the isotype in question to the epitope in question in the first three study visits. Mixed-effects models were chosen to assess the effect of time post infection whilst accounting for the repeated measurement of participants. For each observation *i*, we modeled the antibody response Yi as:

$$Y_i \sim N\left(\alpha_{j[i]} + \beta_1 Time, \sigma^2\right)$$
$$\alpha_j \sim N\left(\mu_{\alpha j}, \sigma^2_{\alpha j}\right), for\ Participant\ j = 1, \dots, J$$

Where β1 is the fixed-effect slope coefficient for *Time* the number of days after the first SARS-Cov-2 PCR+ result was returned that the blood sample was drawn. α_j represents the participant-level normally distributed random intercept. We examined the total explanatory

power (conditional R2) and residual plots to check assumptions (linearity, random distribution of residuals and homoscedasticity) for each model. We also considered models with additional fixed effects for covariates (age, sex, hospitalisation status, and a proxy for overall antibody titre in the Euroimmun IgG assay) and found that the inclusion of these terms did little to improve model fit and did not materially change the conclusions drawn from the modelling about the rate of waning of isotypes for specific epitopes. This suggests that these covariates tend not to greatly effect the rate at which antibodies wane beyond their effects on the starting titre, which is already accounted for in the participant-level random intercept. Models were fit using the lme4 package in R statistical software.

Lasso penalized regression

Examining the response for three antibody isotypes (IgG, IgM, IgA) for eight epitopes and the receptor binding domain, and covariates for sex, age, and days since symptom onset, yields 30 parameters for the 70 Oxford cohort participants: i.e. a high ratio of parameters (p) to subjects (n). We therefore used a penalized regression approach to discriminate the most predictive immunogenic epitopes (reducing the p:n). The least absolute shrinkage and selection operator (Lasso) method was adopted as it allows for variable selection during regularization and can be applied to generalized linear models. In a Bayesian interpretation, Lasso regression can be interpreted as linear (or generalized) regression where the coefficients have Laplace prior distributions (peaked at zero) leading to a tendency for coefficients to shrink to zero. This feature is an advantage over other regularization techniques (e.g. Ridge regression) as it aids interpretability by eliminating less-predictive variables from the model. Since we intended to include age, sex, and days post PCR of sampling, as covariates in subsequent models, we were interested to identify the single most predictive immunogenic epitope for effect size estimation in non-penalized regression models, rather than selecting the optimum regularization parameter and multiple isotype-epitope responses. However, we also examined the AIC for sequential values of the regularization parameter to identify the optimum value and performed sensitivity analyses to examine the approach to variable transformations on the results of selection.

The age variable was log transformed, sex was included as a binary variable, and time post PCR result was coded in days. Because we were comparing different secondary antibodies used at different concentrations simultaneously and because we had limited sample volume (60ul – 100ul) with which to test all isotypes for all epitopes and so had used the ratio of a single dilution (1/50) of serum to a known positive plate control (Technopath positive serum to whole spike S1' subunit) to calculate the arbitrary units of ELISA titre, we interpret these titres as semi-quantitative. The validity of this approach is evidenced by the expected waning in longitudinal responses and the consistency of our results identifying immunodominant antigens with those reported by others. However, titres will not be directly comparable between isotypes due to the issue of different secondary antibodies meaning that these variables required a some form of normalizing transformation. Each sera was used at a dilution of 1/50 and each antigen at 1.25ug/ml which prior experiments had suggested would mean that most subjects with detectable responses were on the linear part of the ELISA response curve, however, those with very high titres will be outwith the upper limit of the linear range of our assay and so discriminating between extreme high titres would be potentially misleading. Therefore, we dichotomized each antigen based on the median response in the whole cohort (n=70) to represent either low (or no) versus high antibody responses. We determined not to include any antibody isotype where <5% of the cohort were responders (which excluded the IgG response to the N2 epitope) to prevent

misleadingly incorporating responses below the lower limit of detection of the assay. We performed a secondary analysis including all variables but dichotomizing at the lower of either: 1/ the lower limit of detection of a response for each epitope-isotype combination based on the mean response of the 50 individual negative controls + 3SDs, or 2/ the median response in the cohort. These two approaches we found to give substantially the same result and the simpler median dichotomization is therefore reported in Fig. 5B due to being easier to interpret.

We performed further sensitivity analyses using a cutoff of the 65th percentile (45/70) rather than the median as the cohort were not a population based random sample of persons infected with SARS-CoV-2, rather essentially were a comparison of an arbitrary number of asymptomatic/mild individuals (n=45) to severe/critical (n=25) individuals. This sensitivity analysis corroborated the prior results highlighting the importance of the M1 IgM response. Lasso regression models were fit using the glmnet package in R statistical software.

Multivariable logistic regression models

After identifying the M1 IgM as the strongest immunological predictor in Lasso models, we fitted three logistic models (estimated using maximum likelihood) without shrinkage to predict COVID-19 disease severity with age and M1 IgM as predictors (Fig. 5C). As above, we log (base 2) transformed age given the well described log-linear association of age and SARS-CoV-2 infection fatality rate. Exponentiated age coefficients can be interpreted as the odds ratio associated with doubling a participant's age, adjusting for the other variables in the model. We dichotomized M1 IgM at the lower of the median value or the lower limit of detection of the assay for the responses to each isotype and each epitope, as before for Lasso regression.

Model 1: $\log \frac{P(Severe)}{1-P(Severe)} = \alpha + \beta_1 DPSO + \beta_2 M1^{hi} + \beta_3 \log(Age) + \beta_4 Sex_{Male}$

Model 2: $\log \frac{P(Severe)}{1-P(Severe)} = \alpha + \beta_1 DPSO + \beta_2 M1^{hi} + \beta_3 \log(Age)$

Model 3: $\log \frac{P(Severe)}{1-P(Severe)} = \alpha + \beta_1 DPSO + \beta_2 M1^{hi}$

Where β1 is the coefficient for days post symptom onset (*DPSO*), β2 is the coefficient associated with a high M1 IgM ($M1^{hi}$), β3 the coefficient for the logarithm (base 2) of age, and β4 the coefficient for male sex (Sex_{male}). We examined the total explanatory power of all three models using Tjur's R2 (ref) and inspected residual plots to ensure assumptions of the model (linearity, random distribution of residuals and homoscedasticity) were not violated. We performed sensitivity analyses as for Lasso penalized regression: using a cutoff at the 65th percentile (45/70) rather than the median, and using the untransformed raw ELISA titre and the log transformed ELISA titres. Sensitivity analyses did not substantially improve model fit or change the interpretation of the model, the coefficients for age, sex, and having a high IgM remained statistically significant, positive, and large.

Dimensionality reduction methods

To reduce the dimensionality of the 8 epitopes + RBD, and 3 antibody isotypes, we employed uniform manifold approximation and projection (UMAP) to represent patterns in two-dimensional space. Antibody titres were log transformed and scaled by the standard deviation of

the response for each peptide. Similar results were observed using unscaled and untransformed data. UMAP were performed using the UMAP package in R statistical software.

Multiple sequence alignments

Multiple sequence alignments were performed using MUSCLE with default parameters. Alignments were manually adjusted where necessary and figures prepared using Snapgene software (Insightful Science), Jalview, Adobe Acrobat and Adobe Illustrator.

Analysis of SARS-CoV-2 variant mutation frequency

Sampling of public sequencing data to investigate the prevalence of mutations in M1 epitopes was performed using tools available at www.nexstrain.org using GISAID data (*91*).

Statistical software

Statistical analysis were performed in R v4.2.0 and RStudio v1.2.5019. A complete list of packages with version numbers are provided in the supplementary materials.

Experimental testing of TI B cell activation hypothesis

Raising affinity matured anti-M1 antibodies in Rabbit

The M1 peptide sythesized and purity determined by HPLC to be used as an immunogen by Cambridge Research Biochemicals under a collaboration agreement (crbdiscovery.com). The final immunogen trimmed the first methionine, and replaced the Glutamine (Q)19 with a cysteine for conjugation to keyhole limpet hemocyanin. This was then used to immunize two rabbits: the first immunization was delivered with Freund's complete adjuvant, and subsequent immunisations with Freunds incomplete adjuvant over 77days. Two animals were immunized, both demonstrated a strong seroconversion with pre-immune IgG ELISA titres 1:<10, and final ELISA titres >1:10000. Blocking antibody used in this study was purified by peptide affinity column, and eluted at acidic pH.

Production and purification of SARS-CoV-2 virus-like particles (VLPs)

HEK293T cells used for VLP production were maintained in DMEM supplemented with 10% FCS, 100µg/µl penicillin, and 100µg/µl streptomycin sulphate. HEK293T cells in T-175 flasks were co-transfected with plasmids for SARS-CoV-2 M gene (18.75µg), E gene (18.75µg)1, and N gene (12.5µg) (gift from Paul Digard) using 100µl Lipofectamine 3000 transfection reagent and 100µl P3000 reagent (Invitrogen, L3000001) according to the manufacturer's instructions. VLPs were harvested from cell culture supernatant 72 h after transfection based on a previously described method (*92*, *93*). Briefly, cell culture supernatant was clarified by centrifugation at 1000xg for 10 min, clarified supernatant was transferred to ultracentrifuge tubes and underlaid with a 20% sucrose cushion using a 4" blunt needle. VLPs were pelleted by centrifugation for 2h at 4°C, 28,000rpm using an SW28 Ti swinging bucket rotor. Supernatant was removed and ultracentrifuge tubes inverted for 5 minutes on paper towel to remove residual supernatant. Pelleted VLPs were resuspended in 200µl of PBS per T-175 flask used for VLP production. VLPs were aliquoted, snap frozen, and stored at -80°C until use.

Protease protection assay to assess VLP integrity

VLPs were assessed for lipid membrane integrity using a protease protection assay. Equal amounts of VLPs were treated with 1% triton-X-100 or 1X Trypsin 1:250 (Gibco) as indicated and incubated at 37°C for 1h. VLPs were then mixed with 4X SDS-PAGE loading buffer and heated at 95°C for 5 min prior to SDS-PAGE and Western blot analysis.

Western Blotting

Proteins were separated by SDS-PAGE and transferred to 0.45µm PVDF membranes. After blocking with 5% skim milk in TBS-T, membranes were incubated with the indicated primary antibodies (0.25µg/ml sheep anti-N or 0.25µg/ml sheep anti-M)1, followed by secondary antibody horseradish peroxidase (HRP)-conjugated rabbit anti-sheep IgG (Santa Cruz Biotechnology, Inc, sc-2924) at 1:10000 dilution. Chemiluminescence was detected using PierceTM ECL Western Blotting Substrate and an iBright FL1500 imager (Thermo Fisher Scientific).

Transmission Electron Microscopy (TEM)

5µl of VLPs were applied to a formvar/carbon supported 3.05mm copper grid (size 200 mesh) for 10 min before blotting off excess material and negative staining with uranyl acetate for 1 min. Excess stain was removed and grids were air dried for 15 min before imaging on a JEOL-1400 Plus TEM. The approximate diameter of VLPs was measured using the ImageJ line selection tool.

Primary B cell culture and stimulation

For the COVID-19 naïve donor experiment, mononuclear cells from peripheral blood were isolated as previously described from three COVID-19 naïve donors (N-01, N-02, N-03) (*94*). Briefly, fresh blood samples from healthy individuals were collected in EDTA tubes. Blood was diluted 1:1 with PBS and layered gently on Ficoll-Paque in SepMATE tubes (StemCell Technologies) followed by density gradient centrifugation. Cells were thoroughly washed and were either freshly stained for flow cytometry or were stored in freezing medium (Cryostor CS10 cell cryopreservation media, Cat. C2874, Sigma-Aldrich) at −150°C., frozen PBMC's were thawed, washed and resuspended in RPMI containing 10% FBS, L-Glutamine, non-essential amino acids, HEPES, and 100U/ml penicillin plus 100ug/ml streptomycin. B cell purification was performed using EasySepTM Human B cell Enrichment Kit (Cat#19054, Stemcell technology) following manufacturer's protocol. $5x10^4$ cells were plated in 96 u-bottom well plate and stimulated with: (i) VLP 1:10 (10ul VLP resuspension in 100ul total culture media); (ii) VLPs 1:500 (0.2ul in 100ul); (iii) R848 1:250 (Cat#tlrl-r848, Invivogen); (iv) CpGB DNA 1:500 (Cat#HC4039, Cambridge Bioscience); (v) CD40L 10 µg/mL (Cat#6245-CL-050, R&D Systems); (vi) detergent treated VLPs, these were as in (i) but with 1% Triton-x-100 added for 30 mins to dissolve lipid-protein structures before having buffer exchanged to remove detergent by passing over 3kDa MWCO spin column for 6x washes. For unstimulated control, cells were in complete media with no additions. Following stimulation, supernatant was collected, and immunoglobulin profiles were analysed using LegendPlex following manufacturer's protocol (Cat#740640, Biolegend).

For the experiment in recently recovered individuals, culture conditions were similar to those above with some adjustments. B cells were isolated immediately from freshly collected

whole blood by incubating whole blood diluted 1:1 in PBS, for 15 mins with 50ul per 10ml RosetteSep™ Human B Cell Enrichment Cocktail, and layering on Lymphoprep™ density gradient media (STEMCELL Technologies) in SepMate™ 50ml tubes, as recommended by the manufacturer. Depletion of CD3 positive cells and enrichment of CD19 positive cells was confirmed as above by flow cytometry. B cells were washed in PBS and pelleted, before being resuspended in RMPI supplemented with 20% FCS, L-Glutamine, 100µg/µl penicillin, and 100µg/µl streptomycin sulphate. Purified B cells were then plated at $5x10^4$ cells per well of a 96-well U-bottom plate before the addition of VLPs for a final dilution of either 1:10 or 1:100. In addition, extra negative control conditions were used: with B cells either (i) untreated (PBS added at 1:10 dilution), (ii) treated with VLPs that had been pre-incubated with 1/500 dilution of a polyclonal anti-M1 rabbit antibody; (iii) a 1:10 dilution of OC43-VLPs. Each condition was tested in technical triplicate for three different B cell donors, with a final well volume of 110µl following addition of VLPs. B cells were cultured for 14 days post-stimulation with cells imaged on day 8 and 14. On day 14 cell culture supernatant was collected and stored at -80°C until use.

Immunofluorescence

293T cells were seeded on poly-L-lysine coated 13mm (#1.5) circular coverslips and grown overnight to 60% confluency in 24 well flat-bottomed plates in complete media as described above. These were then transfected with expression vectors for SARS-CoV-2 M protein, or variants of the M protein, using Lipofectamine3000 as previously described. After 24 hours of expression, coverslips were washed in PBS, fixed in 4% paraformaldehyde for 12 minutes, permeabilised (or not) using 0.2% Triton X-100 in PBS for 7 mins, and washed three times in PBS. Coverslips were then blocked using PBS +4% BSA for 30 minutes, before being incubated with the indicated primary antibodies at 0.5ug/ml diluted in blocking solution overnight at 4^0C (sheep anti-M, anti-E). These were then washed in PBS three times for 5 minutes each, before being incubated with secondary antibodies diluted 1:1000 (rabbit anti-sheep Alexafluor 594) in blocking solution for 1h at room temperature. Coverslips were then washed in PBS three times for 5 minutes each with the final wash containing 50ug/ml DAPI. Epifluorescent images were acquired using a Hamamatsu Orca Flash 4.0 cMOS camera (Hamamatsu, Japan) and a Zeiss Zeiss AxioImager M2 fluorescence microscope with a 100x oil-immersino Plan neofluar/apochromat objective lenses (Carl Zeiss, Cambridge, UK), a Mercury Halide fluorescent light source (Exfo Excite 120, Excelitas Technologies) and Chroma #83000 triple band pass filter set (Chroma Technology Corp., Rockingham, VT) with the single excitation and emission filters installed in motorised filter wheels (Prior Scientific Instruments, Cambridge, UK). Image capture was performed using Micromanager (Version 1.4).

Subjects for PBMC donation

Blood was collected for B cell assays under the ethical approval from the Edinburgh Medical School Research Ethics Committee of the University of Edinburgh (21-EMREC-010). Three healthy controls with no known SARS-CoV-2 history, and prior vaccination were recruited as a convenience sample from volunteers at our research institute. For the recent COVID-19 recovered donors, volunteers were identified by their response to a email enquiry. After collection of informed consent, demographics, and recent SARS-CoV-2 infection, and SARS-CoV-2 vaccination history was collected. Samples were then pseudonymized at source.

Low-resolution automated culture microscopy

Primary B cells were imaged at day 8 and day 14 whilst in 96-well u-bottomed plates in a high-content a custom plate scanning program which allowed for individual well z-plane focus adjustment to optimize focus in the u-bottom flasks. The microscope comprises of a Nikon Eclipse Ti-E inverted microscope (Nikon Instruments UK Ltd, Kingston Upon Thames, UK) using a a 10x phase-contrast objective. Widefield illumination is provided by a CoolLED PE-4000 LED light source (CoolLED Ltd, Andover, UK). Images were acquired with a Photometrics Prime BSI sCMOS camera (Teledyne Photometrics, 3440 E. Britannia Drive, Suite 100, Tucson, AZ 85706). Conditional imaging was setup and controlled through Nikon Jobs.

References and Notes:

1. M. F. Flajnik, Comparative analyses of immunoglobulin genes: surprises and portents. *Nat. Rev. Immunol.* **2**, 688–698 (2002).
2. T. Kurosaki, K. Kometani, W. Ise, Memory B cells. *Nat. Rev. Immunol.* **15**, 149–59 (2015).
3. E. Y. Wang *et al.*, Diverse functional autoantibodies in patients with COVID-19. *Nature*. **595**, 283–288 (2021).
4. S. F. Wang *et al.*, Antibody-dependent SARS coronavirus infection is mediated by antibodies against spike proteins. *Biochem. Biophys. Res. Commun.* **451**, 208–214 (2014).
5. A. T. Huang *et al.*, A systematic review of antibody mediated immunity to coronaviruses: kinetics, correlates of protection, and association with severity. *Nat. Commun.* **11**, 1–16 (2020).
6. W. G. Laver *et al.*, Epitopes on protein antigens: misconceptions and realities. *Cell*. **61**, 553–556 (1990).
7. M. H. V. Van Regenmortel, What is a b-cell epitope? *Methods Mol. Biol.* **524**, 3–20 (2009).
8. J. A. Schroer *et al.*, Mapping epitopes on the insulin molecule using monoclonal antibodies. *Eur. J. Immunol.* **13**, 693–700 (1983).
9. P. Haste Andersen, M. Nielsen, O. Lund, Prediction of residues in discontinuous B-cell epitopes using protein 3D structures. *Protein Sci.* **15**, 2558–2567 (2006).
10. M. O'Driscoll *et al.*, Age-specific mortality and immunity patterns of SARS-CoV-2. *Nature*. **590**, 140–145 (2021).
11. T. Zohar, G. Alter, Dissecting antibody-mediated protection against SARS-CoV-2. *Nat. Rev. Immunol.* **20** (2020), pp. 392–394.
12. P. Bastard *et al.*, Autoantibodies against type I IFNs in patients with life-threatening COVID-19. *Science (80-.).* **370** (2020), doi:10.1126/SCIENCE.ABD4585/SUPPL_FILE/ABD4585_MDAR-REPRODUCIBILITYCHECKLIST.PDF.
13. J. A. Marsh, Buried and accessible surface area control intrinsic protein flexibility. *J. Mol. Biol.* **425**, 3250–3263 (2013).

14. J. A. Marsh, S. A. Teichmann, Relative solvent accessible surface area predicts protein conformational changes upon binding. *Structure*. **19**, 859–867 (2011).

15. J. A. Marsh *et al.*, Protein Complexes Are under Evolutionary Selection to Assemble via Ordered Pathways. *Cell*. **153**, 461 (2013).

16. F. Yasui *et al.*, Prior Immunization with Severe Acute Respiratory Syndrome (SARS)-Associated Coronavirus (SARS-CoV) Nucleocapsid Protein Causes Severe Pneumonia in Mice Infected with SARS-CoV. *J. Immunol.* **181**, 6337–6348 (2008).

17. E. Shrock *et al.*, Viral epitope profiling of COVID-19 patients reveals cross-reactivity and correlates of severity. *Science (80-.).* **370** (2020), doi:10.1126/science.abd4250.

18. C. R. Zamecnik *et al.*, ReScan, a Multiplex Diagnostic Pipeline, Pans Human Sera for SARS-CoV-2 Antigens. *Cell Reports Med.* **1**, 100123 (2020).

19. H. Wang *et al.*, SARS-CoV-2 Proteome Microarray for Mapping COVID-19 Antibody Interactions at Amino Acid Resolution. *ACS Cent. Sci.* **6**, 2238–2249 (2020).

20. F. Obermeyer *et al.*, Analysis of 6.4 million SARS-CoV-2 genomes identifies mutations associated with fitness. *Science (80-.).* (2022), doi:10.1126/SCIENCE.ABM1208.

21. N. Baumgarth *et al.*, B-1 and B-2 Cell–Derived Immunoglobulin M Antibodies Are Nonredundant Components of the Protective Response to Influenza Virus Infection. *J. Exp. Med.* **192**, 271–280 (2000).

22. S. R. Khan *et al.*, Determinants and Reference Ranges of Serum Immunoglobulins in Middle-Aged and Elderly Individuals: a Population-Based Study. *J. Clin. Immunol.* **41**, 1902 (2021).

23. C. E. Buckley, F. C. Dorsey, The Effect of Aging on Human Serum Immunoglobulin Concentrations. *J. Immunol.* **105** (1970).

24. L. Piccoli *et al.*, Mapping neutralizing and immunodominant sites on the SARS-CoV-2 spike receptor-binding domain by structure-guided high-resolution serology. *Cell*. **183**, 1024-1042.e21 (2020).

25. A. Addetia *et al.*, Neutralizing antibodies correlate with protection from SARS-CoV-2 in humans during a fishery vessel outbreak with a high attack rate. *J. Clin. Microbiol.* **58** (2020), doi:10.1128/JCM.02107-20.

26. B. Boson *et al.*, The SARS-CoV-2 envelope and membrane proteins modulate maturation and retention of the spike protein, allowing assembly of virus-like particles. *J. Biol. Chem.* **296**, 100111 (2021).

27. Y. L. Siu *et al.*, The M, E, and N Structural Proteins of the Severe Acute Respiratory Syndrome Coronavirus Are Required for Efficient Assembly, Trafficking, and Release of Virus-Like Particles. *J. Virol.* **82**, 11318–11330 (2008).

28. B. W. Neuman *et al.*, A structural analysis of M protein in coronavirus assembly and morphology. *J. Struct. Biol.* **174**, 11 (2011).

29. Z. Ke *et al.*, Structures and distributions of SARS-CoV-2 spike proteins on intact virions. *Nat. 2020 5887838*. **588**, 498–502 (2020).

30. W. Pezeshkian *et al.*, Molecular architecture and dynamics of SARS-CoV-2 envelope by integrative modeling. *Structure* (2023), doi:https://doi.org/10.1016/j.str.2023.02.006.

31. J. J. Mond *et al.*, T cell independent antigens. *Curr. Opin. Immunol.* **7**, 349–354 (1995).

32. T. A. Y. Shih, M. Roederer, M. C. Nussenzweig, Role of antigen receptor affinity in T cell-independent antibody responses in vivo. *Nat. Immunol.* **3**, 399–406 (2002).

33. B. A. Heesters *et al.*, Antigen Presentation to B Cells. *Trends Immunol.* **37**, 844–854 (2016).

34. D. Paus *et al.*, Antigen recognition strength regulates the choice between extrafollicular plasma cell and germinal center B cell differentiation. *J. Exp. Med.* **203**, 1081–1091 (2006).

35. C. García de Vinuesa *et al.*, T-independent type 2 antigens induce B cell proliferation in multiple splenic sites, but exponential growth is confined to extrafollicular foci, doi:10.1002/(SICI)1521-4141(199904)29:04.

36. J. A. Roco *et al.*, Class-Switch Recombination Occurs Infrequently in Germinal Centers. *Immunity*. **51**, 337-350.e7 (2019).

37. T. V. Obukhanych, M. C. Nussenzweig, T-independent type II immune responses generate memory B cells. *J. Exp. Med.* **203**, 305–310 (2006).

38. M. Brüggemann, K. Rajewsky, Regulation of the antibody response against hapten-coupled erythrocytes by monoclonal antihapten antibodies of various isotypes. *Cell. Immunol.* **71**, 365–373 (1982).

39. R. A. Herlands *et al.*, T cell-independent and toll-like receptor-dependent antigen-driven activation of autoreactive B cells. *Immunity*. **29**, 249–260 (2008).

40. T. Fehr *et al.*, T cell-independent type I antibody response against B cell epitopes expressed repetitively on recombinant virus particles. *Proc. Natl. Acad. Sci. U. S. A.* **95**, 9477–9481 (1998).

41. R. S. Thwaites *et al.*, Inflammatory profiles across the spectrum of disease reveal a distinct role for GM-CSF in severe COVID-19. **6** (2021) (available at https://www.science.org/doi/full/10.1126/sciimmunol.abg9873).

42. N. Kaneko *et al.*, Loss of Bcl-6-Expressing T Follicular Helper Cells and Germinal Centers in COVID-19. *Cell*. **183**, 143-157.e13 (2020).

43. S. De Biasi *et al.*, Expansion of plasmablasts and loss of memory B cells in peripheral blood from COVID-19 patients with pneumonia. *Eur. J. Immunol.* **50**, 1283–1294 (2020).

44. J. P. Bernardes *et al.*, Longitudinal Multi-omics Analyses Identify Responses of Megakaryocytes, Erythroid Cells, and Plasmablasts as Hallmarks of Severe COVID-19. *Immunity*. **53**, 1296-1314.e9 (2020).

45. T. Takai *et al.*, Augmented humoral and anaphylactic responses in Fc gamma RII-deficient mice. *Nature*. **379**, 346–349 (1996).

46. P. H. Brodeur, H. H. Wortis, Regulation of thymus-independent responses: unresponsiveness to a second challenge of TNP-Ficoll is mediated by hapten-specific antibodies. *J. Immunol.* **125** (1980).

47. A. M. Syed *et al.*, Omicron mutations enhance infectivity and reduce antibody neutralization of SARS-CoV-2 virus-like particles. *Proc. Natl. Acad. Sci. U. S. A.* **119**, e2200592119 (2022).

48. M. Whitaker *et al.*, Persistent COVID-19 symptoms in a community study of 606,434 people in England. *Nat. Commun.* **13** (2022), doi:10.1038/S41467-022-29521-Z.

49. A. J. Morrow *et al.*, A multisystem, cardio-renal investigation of post-COVID-19 illness. *Nat. Med. 2022*, 1–11 (2022).

50. Z. Al-Aly, Y. Xie, B. Bowe, High-dimensional characterization of post-acute sequelae of COVID-19. *Nature*. **594**, 259–264 (2021).

51. C. Gaebler *et al.*, Evolution of antibody immunity to SARS-CoV-2. *Nature*. **591**, 639–644 (2021).

52. S. Martin *et al.*, SARS-CoV-2 integral membrane proteins shape the serological responses of patients with COVID-19. *iScience*. **24**, 103185 (2021).

53. H. Yao *et al.*, Molecular Architecture of the SARS-CoV-2 Virus. *Cell*. **183**, 730–738 (2020).

54. M. J. Mina *et al.*, Measles virus infection diminishes preexisting antibodies that offer protection from other pathogens. *Science*. **366**, 599–606 (2019).

55. P. Jörrißen *et al.*, Antibody Response to SARS-CoV-2 Membrane Protein in Patients of the Acute and Convalescent Phase of COVID-19. *Front. Immunol.* **12**, 679841 (2021).

56. Y. R. Carrasco, F. D. Batista, B cell recognition of membrane-bound antigen: an exquisite way of sensing ligands. *Curr. Opin. Immunol.* **18**, 286–291 (2006).

57. M. F. Bachmann, H. Hengartner, R. M. Zinkernagel, T helper cell-independent neutralizing B cell response against vesicular stomatitis virus: role of antigen patterns in B cell induction? *Eur. J. Immunol.* **25**, 3445–3451 (1995).

58. E. Szomolanyi-Tsuda *et al.*, Antiviral T-cell-independent type 2 antibody responses induced in vivo in the absence of T and NK cells. *Virology*. **280**, 160–168 (2001).

59. E. A. Leadbetter *et al.*, Chromatin-IgG complexes activate B cells by dual engagement of IgM and Toll-like receptors. *Nature*. **416**, 603–607 (2002).

60. E. J. Pone *et al.*, BCR-signalling synergizes with TLR-signalling for induction of AID and immunoglobulin class-switching through the non-canonical NF-κB pathway. *Nat. Commun.* **3**, 767 (2012).

61. D. R. Milich, A. Mclachlan, The nucleocapsid of hepatitis B virus is both a T-cell-independent and a T-cell-dependent antigen. *Science*. **234**, 1398–1401 (1986).

62. P. Bastard *et al.*, Autoantibodies neutralizing type I IFNs are present in ~4% of uninfected individuals over 70 years old and account for ~20% of COVID-19 deaths. *Sci. Immunol.* **6**, 4340–4359 (2021).

63. J. Troya *et al.*, Neutralizing autoantibodies to type I IFNs in> 10\% of patients with severe COVID-19 pneumonia hospitalized in Madrid, Spain. *J. Clin. Immunol.* **41**, 914–922 (2021).

64. X. Solanich *et al.*, Pre-existing Autoantibodies Neutralizing High Concentrations of Type I Interferons in Almost 10% of COVID-19 Patients Admitted to Intensive Care in Barcelona. *J. Clin. Immunol.* **41** (2021) (available at /pmc/articles/PMC8475877/).

65. A. Chauvineau-Grenier *et al.*, Autoantibodies Neutralizing Type I Interferons in 20% of

COVID-19 Deaths in a French Hospital. *J. Clin. Immunol.* **42**, 459–470 (2022).

66. D. L. Sykes *et al.*, Post-COVID-19 Symptom Burden: What is Long-COVID and How Should We Manage It? *Lung*. **199**, 113–119 (2021).

67. H. Nishiura, N. M. Linton, A. R. Akhmetzhanov, Serial interval of novel coronavirus (COVID-19) infections. *Int. J. Infect. Dis.* (2020), doi:10.1016/j.ijid.2020.02.060.

68. S. Alexander, J. H. Elder, Carbohydrate dramatically influences immune reactivity of antisera to viral glycoprotein antigens. *Science*. **226**, 1328–1330 (1984).

69. K. V. Holmes, E. W. Doller, L. S. Sturman, Tunicamycin resistant glycosylation of coronavirus glycoprotein: demonstration of a novel type of viral glycoprotein. *Virology*. **115**, 334–344 (1981).

70. C. A. M. De Haan *et al.*, The glycosylation status of the murine hepatitis coronavirus M protein affects the interferogenic capacity of the virus in vitro and its ability to replicate in the liver but not the brain. *Virology*. **312**, 395 (2003).

71. M. M. Shafer *et al.*, *medRxiv*, in press, doi:10.1101/2022.10.28.22281553.

72. D.-Y. Chen *et al.*, Role of spike in the pathogenic and antigenic behavior of SARS-CoV-2 BA. 1 Omicron. *bioRxiv*, 2010–2022 (2022).

73. L. Y. R. Wong, S. Perlman, Immune dysregulation and immunopathology induced by SARS-CoV-2 and related coronaviruses — are we our own worst enemy? *Nat. Rev. Immunol.* **22** (2022), pp. 47–56.

74. M. M. Lamers, B. L. Haagmans, SARS-CoV-2 pathogenesis. *Nat. Rev. Microbiol.* **20** (2022), pp. 270–284.

75. M. Merad *et al.*, The immunology and immunopathology of COVID-19. *Science (80-.).* **375** (2022), pp. 1122–1127.

76. D. A. Dorward *et al.*, Tissue-specific immunopathology in fatal COVID-19. *Am. J. Respir. Crit. Care Med.* **203**, 192–201 (2021).

77. E. Y. Wang *et al.*, Diverse Functional Autoantibodies in Patients with COVID-19. *Nature*, 1–6 (2021).

78. P. Bastard *et al.*, Autoantibodies against type I IFNs in patients with life-threatening COVID-19. *Science (80-.).* **370** (2020), doi:10.1126/science.abd4585.

79. L. A. Kelley *et al.*, The Phyre2 web portal for protein modeling, prediction and analysis. *Nat. Protoc. 2015 106*. **10**, 845–858 (2015).

80. L. Heo, H. Lee, C. Seok, GalaxyRefineComplex: Refinement of protein-protein complex model structures driven by interface repacking. *Sci. Rep.* **6** (2016), doi:10.1038/SREP32153.

81. M. D. Winn *et al.*, Overview of the CCP4 suite and current developments. *Acta Crystallogr. Sect. D Biol. Crystallogr.* **67** (2011), pp. 235–242.

82. M. C. Jespersen *et al.*, BepiPred-2.0: improving sequence-based B-cell epitope prediction using conformational epitopes. *Nucleic Acids Res.* **45**, W24–W29 (2017).

83. C. Zhou *et al.*, SEPPA 3.0-enhanced spatial epitope prediction enabling glycoprotein antigens. *Nucleic Acids Res.* **47**, W388–W394 (2019).

84. S. Liang *et al.*, EPSVR and EPMeta: Prediction of antigenic epitopes using support vector regression and multiple server results. *BMC Bioinformatics*. **11**, 1–6 (2010).

85. M. J. Sweredoski, P. Baldi, PEPITO: improved discontinuous B-cell epitope prediction using multiple distance thresholds and half sphere exposure. *Bioinformatics*. **24**, 1459–1460 (2008).

86. M. Kurcinski *et al.*, CABS-flex standalone: A simulation environment for fast modeling of protein flexibility. *Bioinformatics*. **35**, 694–695 (2019).

87. J. Ponomarenko *et al.*, ElliPro: A new structure-based tool for the prediction of antibody epitopes. *BMC Bioinformatics*. **9**, 1–8 (2008).

88. M. A. Lomize *et al.*, OPM database and PPM web server: resources for positioning of proteins in membranes. *Nucleic Acids Res.* **40**, D370–D376 (2012).

89. E. F. Pettersen *et al.*, UCSF ChimeraX: Structure visualization for researchers, educators, and developers. *Protein Sci.* **30**, 70–82 (2021).

90. F. Muecksch *et al.*, Longitudinal serological analysis and neutralizing antibody levels in coronavirus disease 2019 convalescent patients. *J. Infect. Dis.* **223**, 389–398 (2021).

91. S. Khare *et al.*, GISAID's Role in Pandemic Response. *China CDC Wkly*. **3**, 1049 (2021).

92. C. B. Plescia *et al.*, SARS-CoV-2 viral budding and entry can be modeled using BSL-2 level virus-like particles. *J. Biol. Chem.* **296** (2021), doi:10.1074/JBC.RA120.016148.

93. A. M. Syed *et al.*, Rapid assessment of SARS-CoV-2--evolved variants using virus-like particles. *Science (80-.).* **374**, 1626–1632 (2021).

94. H. A. Shuwa *et al.*, Alterations in T and B cell function persist in convalescent COVID-19 patients. *Med (New York, N.Y.).* **2**, 720-735.e4 (2021).

Acknowledgments: We are grateful to Professors David Gray and members of the Gilbert Lab and MRC Human Genetics Unit for useful discussions throughout the project. We are grateful to Scott Neilson of the Edinburgh Genome Foundry for assistance with robotic cloning pipelines. We are grateful to the staff of the Scottish National Blood Transfusion Service Microbiology Reference Unit staff for provision of samples from Scottish blood donors. This research was conducted with material produced with the assistance of the Edinburgh Genome Foundry, a synthetic biology research facility specialising in the assembly of large DNA fragments at the University of Edinburgh. We are also grateful to the staff of the IGC, advanced imaging department, for technical assistance particularly Matt Pearson.

Members of the Manchester Coronavirus Immune Response and Clinical Outcomes (CIRCO) consortium: Rohan Ahmed, Miriam Avery, Katharine Birchall, Evelyn Charsley, Alistair Chenery, Christine Chew, Richard Clark, Emma Connolly, Karen Connolly, Simon Dawson, Laura Durrans, Hannah Durrington, Jasmine Egan, Kara Filbey, Claire Fox, Helen Francis, Miriam Franklin, Susannah Glasgow, Nicola Godfrey, Kathryn J. Gray, Seamus Grundy, Jacinta Guerin, Pamela Hackney, Chantelle Hayes, Emma Hardy, Jade Harris, Anu John, Bethany Jolly, Verena Kästele, Gina Kerry, Sylvia Lui, Lijing Lin, Alex G. Mathioudakis, Joanne Mitchell, Clare Moizer, Katrina Moore, Stuart Moss, Syed Murtuza Baker, Rob Oliver, Grace Padden, Christina Parkinson, Michael Phuycharoen, Ananya Saha, Barbora Salcman, Nicholas A. Scott,

Seema Sharma, Jane Shaw, Joanne Shaw, Elizabeth Shepley, Lara Smith, Simon Stephan, Ruth Stephens, Gael Tavernier, Rhys Tudge, Louis Wareing, Roanna Warren, Thomas Williams, Lisa Willmore, and Mehwish Younas.

Funding:

For the purpose of open access, the author has applied a Creative Commons Attribution (CC BY) licence to any Author Accepted Manuscript version arising from this submission.

PKAK. is supported by a ECAT-Wellcome fellowship (223058/Z/21/Z).

NG is supported by MRC (MC_UU_00007/13).

JAM is a Lister Institute Research Fellow.

Lifearc, UKRI, Medical Research Scotland provided funding for development of the method.

The long COVID study was funded by the chief Scientist Office Scotland.

The CIRCO (Manchester) study was funded by the Wellcome Trust (202865/Z/16/Z).

The Oxford cohort was funded by the UK Department of Health and Social Care as part of the PITCH (Protective Immunity from T cells to Covid-19 in Health workers) Consortium, UKRI as part of "Investigation of proven vaccine breakthrough by SARS-CoV-2 variants in established UK healthcare worker cohorts: SIREN consortium & PITCH Plus Pathway" MR/W02067X/1, with contributions from UKRI/NIHR through the UK Coronavirus Immunology Consortium (UK-CIC), the Huo Family Foundation and The National Institute for Health Research (UKRIDHSC COVID-19 Rapid Response Rolling Call, Grant Reference Number COV19-RECPLAS) and the UK Vaccine Taskforce via NIHR grant to support the running of the Oxford ChAdOx1 nCoV-19 vaccine trial paid to the University of Oxford.

JK was funded by UKRI (MR/W020629/1)

E.B. and P.K. are NIHR Senior Investigators and P.K. is funded by WT109965MA. S.J.D. is funded by an NIHR Global Research Professorship (NIHR300791).

Author contributions:

Conceptualization: PKAK, DJK, JM, NG

Methodology: PKAK, CD, DJK, DC, RK, KL, MM, JM, NG

Computational/bioinformatic analyses: PKAK, MB, OF, LG, JM

Laboratory experiments: PKAK, CD, RC, RS, BP, KL, OF, SB, RK, DJK, NG

Edinburgh cohort: HW, SJ, KT

Oxford cohort: AM, JK, PK, EB, SD, CD, TL, AP

Manchester cohort: MM, TH

Long Covid cohort: AC, LMcW

Synthetic biology pipeline: PKAK, DJK, JG, SN, RF, NG

Statistical analyses: PKAK

Visualization: PKAK, MB

Funding acquisition: PKAK, DJK, TL, PK, EB, SD, KT, JK, AP, JM, NG

Project administration: PKAK, OF, CD, TL, PK, EB, SD, JK, AP, MM, TH, SJ, KT, AC, NG

Supervision: TL, JK, PK, EB, SD, AP, TH, KT, SR, DC, JM, NG

Writing – original draft: PKAK

Writing – review & editing: PKAK, CD, MB, AP, JK, AC, DJK, JAM, NG

All authors reviewed and approved the submitted manuscript.

Competing interests:

PKAK, DJK, JAM, and NG are inventors on a preliminary application for a patent filed 9th December 2021 by University of Edinburgh titled "Thermodynamic prediction, synthesis and prioritisation of immunogenic peptides" and have no other competing interests. AC is a paid editor of JNNP, unpaid president of functional neurological disorders society and gives independent testimony in court on a range of neuropsychiatric subjects on a roughly 50% claimant 50% defender split. LMcW is unpaid as a secretary of British Neuropsychiatry Association and gives independent testimony on court on a range of neuropsychiatric subjects. TL is named as an inventor on a patent application for a vaccine against SARS CoV-2 for an unrelated project. TL was a consultant to Vaccitech for an unrelated project. AJP is chair of the UK Department of Health and Social Care's Joint Committee on Vaccination and Immunisation but does not participate in the JCVI COVID19 committee. He was previously a member of WHO's SAGE. The University of Oxford has a partnership with AstraZeneca for the development of COVID19 vaccines. Other authors declare that they have no competing interests.

Data and materials availability: All data necessary are available in the text or the supplementary materials. Code to reproduce the analyses in the paper can be accessed from the first author's GitHub project repository (github.com/PKKearns/SARS2_Antibody_Profiling_Paper). Materials generated during the course of this study: aliquots of purified GST-peptide fusion proteins for the prioritized peptides and bacterial/mammalian expression vectors are available on request.

Supplementary Figures and Tables (Separate Document):

Figs. S1 to S21

Tables S1 to S9

Data S1 to S4